Commun. Comput. Phys.
doi: 10.4208/cicp.020515.250716a

Vol. **21**, No. 2, pp. 313-357
February 2017

The Landau-Zener Transition and the Surface Hopping Method for the 2D Dirac Equation for Graphene

Ali Faraj[1,2] and Shi Jin[3,4,*]

[1] *Institute of Natural Sciences, Shanghai Jiao Tong University, Shanghai 200240, P.R. China.*
[2] *Grenoble INP, ESISAR, 26902 Valence Cedex 9, France.*
[3] *Department of Mathematics, Institute of Natural Sciences, MOE-LSEC and SHL-MAC, Shanghai Jiao Tong University, Shanghai 200240, P.R. China.*
[4] *Department of Mathematics, University of Wisconsin, Madison, WI 53706, USA.*

Received 2 May 2015; Accepted (in revised version) 25 July 2016

Abstract. A Lagrangian surface hopping algorithm is implemented to study the two dimensional massless Dirac equation for Graphene with an electrostatic potential, in the semiclassical regime. In this problem, the crossing of the energy levels of the system at Dirac points requires a particular treatment in the algorithm in order to describe the quantum transition—characterized by the Landau-Zener probability—between different energy levels. We first derive the Landau-Zener probability for the underlying problem, then incorporate it into the surface hopping algorithm. We also show that different asymptotic models for this problem derived in [O. Morandi, F. Schurrer, J. Phys. A: Math. Theor. 44 (2011) 265301] may give different transition probabilities. We conduct numerical experiments to compare the solutions to the Dirac equation, the surface hopping algorithm, and the asymptotic models of [O. Morandi, F. Schurrer, J. Phys. A: Math. Theor. 44 (2011) 265301].

AMS subject classifications: 35Q41, 37M05, 65M70, 65Z05, 81-08, 81Q20, 81V99

Key words: Dirac equation, Wigner transform, semiclassical model, band crossing, Landau-Zener formula, surface hopping algorithm, spectral methods.

1 Introduction

We are interested in the description of the transport of electrons in a single graphene layer. This material is a two-dimensional flat monolayer of carbon atoms which displays unusual and interesting electronic properties arising from the bi-conically shaped Fermi

*Corresponding author. *Email addresses:* ali.faraj@esisar.grenoble-inp.fr (A. Faraj), jin@math.wisc.edu (S. Jin)

surfaces near the Brillouin zone corners (Dirac points). The electrons propagate as massless Dirac Fermions moving with the Fermi velocity v_F, which is 300 times smaller than the speed of light $v_F \approx \frac{c}{300} \approx 10^6 m.s^{-1}$, and their behavior reproduces the physics of quantum electrodynamics but at much smaller energy scale. Although this model has been studied for a long time, see [5] for a bibliography, it has remained theoretical until the work of [32] where the graphene was produced for the first time. After these results, the interest of researchers on this material has shown a remarkable increase including applications in carbon-based electronic devices [26] and numerical simulations, see e.g. [12] and references therein.

In this paper, we will consider a model of a two-dimensional Dirac equation [2,5,31] of a graphene sheet in the presence of an external potential. This model consists of a small parameter h directly related to the Planck constant. We are interested in the design of an efficient numerical method—the surface hopping method—for the graphene Dirac equation in the semiclassical regime where $h \ll 1$. In this regime, the solution of the Dirac equation is highly oscillatory thus a huge computational cost is required to give accurate wave functions or physical observables for either finite difference methods [4,16] or time-splitting spectral method [18], since one needs to resolve the high frequency both spatially and temporally.

The development of efficient numerical methods for the related Schrödinger equation in the semiclassical regime has motivated many works in the last decade, see the review paper [20] and references therein. In the semiclassical regime, one often uses asymptotic analysis, such as the WKB analysis and the Wigner transform to help to reduce the computational costs and to develop efficient computational methods based on the asymptotic models. In the framework of Wigner transform, the idea is to construct a measure on the phase space, called the Wigner measure, when $h \to 0$, to obtain the physical observables (such as density, flux, and energy) with a computational cost far less than a direct quantum simulation. When the gap between different energy levels is of order one (the so-called *adiabatic* case), the Wigner measure technique provides a simple description of the motion: it can be well approximated by a fully diagonalized system, one classical Liouville equation for each energy level [13]. However, in the graphene Dirac equation, the energy levels *cross* at the Dirac points, where *non-adiabatic* transfers are observed and the particles can tunnel from one band to the other. The standard Wigner approach then needs to be revised to describe the non-adiabatic phenomena.

One of the widely used approaches to simulate the non-adiabatic dynamics is the surface hopping method initially proposed by Tully and Preston [39] as an efficient computational method to go beyond the classical Born-Oppenheimer approximation. This method is widely used in chemistry and molecular dynamics, see for examples [7,35,38, 39]. The basic idea is to combine classical transport of the system on individual potential energy surfaces with instantaneous transitions from one energy surface to the other. The transition rates for this band-to-band hopping are given by the well known Landau-Zener formula [40]. From the mathematical point of view, the first rigorous analysis of non-adiabatic transfer using Landau-Zener formula dates back to Hagedorn [15]. More

recently, the Wigner measure techniques for separated energy levels have been extended in [9] and [10] to systems presenting band crossing. The proof is based on microlocal analysis to justify the Landau-Zener formula. Departing from the results in [9] and [10], a rigorous surface hopping algorithm in the Wigner picture was proposed in [25] for time-dependent two-level Schrödinger systems with conically intersecting eigenvalues and implemented numerically in the Lagrangian formulation in [24]. The corresponding Eulerian numerical scheme was proposed in [23] by formulating the hopping mechanism as an interface condition which is then built into the numerical flux for solving the underlying Liouville equation for each energy level.

In the present article we give a Lagrangian surface hopping algorithm for the graphene Dirac equation similar to the algorithm in [24]. First, it is a classical result that the Wigner transform leads to two decoupled classical Liouville equations for each energy level, under the adiabatic assumption [13]. At the Dirac points where non-adiabatic transition occurs, we first derive the Landau-Zener formula, and then incorporate it into the surface hopping algorithm. We also show that a reduced asymptotic model developed in [30] could give incorrect transition probability. We then compare through several numerical examples the solutions of the Dirac equation (solved by the time-splitting spectral method), the surface hopping algorithm and the asymptotic models of [30]. Our numerical results show that, when there is no wave interference, the surface hopping algorithm indeed gives the correct non-adiabatic transition at Dirac points, with a much greater computational efficiency compared with the simulations based on solving directly the Dirac equation.

The article is organized as follows: in Section 2 we give the graphene Dirac equation and its semiclassical limit via the Wigner transform in the adiabatic case. We give some examples of potentials to show that non-adiabatic transition is indeed possible. In Section 3, we derive the Landau-Zener transition probability for the graphene Dirac equation. The surface hopping algorithm is given in Section 4. In Section 5, we study the asymptotic models introduced in [30] and show that a reduced model could give the incorrect transition probability. Numerical results are given in Section 6 for comparisons of different models. For reader's convenience we give the time-splitting spectral method of the Dirac equation in Appendix A.

2 Quantum transport in graphene and the Wigner measure

We consider the description of the transport of electrons in a single graphene layer in the presence of an external potential. Following [2, 5, 31], it is modelled by the two dimensional Dirac equation:

$$\begin{cases} i\hbar\partial_t\psi = [-i\hbar v_F\sigma_1\partial_{x_1} - i\hbar v_F\sigma_2\partial_{x_2} + qV]\,\psi, & t\in IR,\ x\in IR^2, \\ \psi(0,x) = \psi_I(x), & x\in IR^2, \end{cases} \tag{2.1}$$

where $\hbar$ is the reduced Planck constant, v_F is the Fermi velocity, q is the elementary charge of the electron and $V(x)\in IR$ is the electric potential. The Pauli matrices σ_1,σ_2 are given

by:

$$\sigma_1=\begin{pmatrix}0&1\\1&0\end{pmatrix},\quad \sigma_2=\begin{pmatrix}0&-i\\i&0\end{pmatrix}.$$

The initial wave function $\psi_I(x)\in\mathbb{C}^2$ is normalized such that:

$$\int_{IR^2}|\psi_I(x)|^2dx=1 \tag{2.2}$$

and, using the mass conservation, the wave function $\psi(t,x)\in\mathbb{C}^2$ satisfies

$$\int_{IR^2}|\psi(t,x)|^2dx=1, \tag{2.3}$$

where t, $x=(x_1,x_2)$ are the time and space variables respectively. We consider the system (2.1) in the semiclassical regime. For this purpose, we rewrite the equations such that there remains only one dimensionless parameter h. Proceeding as in [36], we change the variables to dimensionless variables as follows

$$t\to t/T_0,\quad x\to x/L \tag{2.4}$$

and define

$$u_I(x)=L\psi_I(Lx),\quad u(t,x)=L\psi(T_0t,Lx), \tag{2.5}$$

where L is a reference length and $T_0=L/v_F$. We remark that $u_I(x)$ and $u(t,x)$ are chosen such that the change of variable preserves the normalization (2.2) and (2.3). Plugging (2.5) into (2.1), and dividing by the reference energy mv_F^2 where m is the effective mass of the electron, one gets the dimensionless graphene Dirac equation:

$$\begin{cases} ih\partial_t u=[-ih\sigma_1\partial_{x_1}-ih\sigma_2\partial_{x_2}+U]u, & t\in IR,\ x\in IR^2,\\ u(0,x)=u_I(x), & x\in IR^2, \end{cases} \tag{2.6}$$

where

$$h=\frac{\hbar}{mv_FL} \tag{2.7}$$

is a small dimensionless parameter and $U(x)$ is the dimensionless potential defined by

$$U(x)=\frac{q}{mv_F^2}V(Lx).$$

We will consider the solution of (2.6) in the limit $h\to 0$.

Non-adiabatic transfer happens at the Dirac points which are the crossing points of the eigenvalues of the symbol related to (2.6). To be more precise, we consider the complex 2×2-matrix-valued symbol:

$$P_0(x,\xi)=B(\xi)+U(x)I,\quad (x,\xi)\in IR^2_x\times IR^2_\xi, \tag{2.8}$$

where I is the 2×2 identity matrix, $B(\xi)$ is given by

$$B(\xi)=\xi_1\sigma_1+\xi_2\sigma_2=\begin{pmatrix} 0 & \xi_1-i\xi_2 \\ \xi_1+i\xi_2 & 0 \end{pmatrix},\quad \xi\in IR^2,$$

and $U\in C^\infty(IR^2,IR)$ is such that $\forall\beta\in IN^2$ there is a constant $C_\beta>0$ verifying:

$$\left|\partial_x^\beta U(x)\right|\leq C_\beta,\quad \forall x\in IR^2.$$

An easy computation shows that the matrix $B(\xi)$ has eigenvalues $\pm|\xi|$ with corresponding orthonormal set of eigenvectors given by

$$\chi_\pm(\xi)=\frac{1}{\sqrt{2}}\left(1,\pm\frac{\xi_1+i\xi_2}{|\xi|}\right)^T. \tag{2.9}$$

We remark that P_0 is a 2×2 matrix with coefficients in $S^1(IR^2\times IR^2)$, where $S^1(IR^2\times IR^2)$ is the set of all $p\in C^\infty(IR^2\times IR^2)$ such that $\forall\beta,\gamma\in IN^2$ there is a constant $C_{\beta,\gamma}>0$ verifying:

$$\left|\partial_x^\beta\partial_\xi^\gamma p(x,\xi)\right|\leq C_{\beta,\gamma}(1+|\xi|)^{1-|\gamma|},\quad \forall(x,\xi)\in IR^2\times IR^2$$

(see [17] for more details about this definition). Moreover, the Dirac equation (2.6) can be rewritten as:

$$\begin{cases} ih\partial_t u^h=P_0(x,hD)u^h, & t\in IR,\\ u^h(0)=u_I^h, \end{cases} \tag{2.10}$$

where $P_0(x,hD)$ is the Weyl operator defined for $u\in\mathbb{C}_0^\infty(IR^2)^2$ by the integral:

$$P_0(x,hD)u(x)=\frac{1}{(2\pi)^2}\int_{IR^2_\xi}\int_{IR^2_y}P_0\left(\frac{x+y}{2},h\xi\right)u(y)e^{i(x-y).\xi}d\xi dy, \tag{2.11}$$

and $D=-i\partial_x$. The operator $P_0(x,hD)$ is essentially self-adjoint on the Hilbert space $\mathcal{H}=L^2(IR^2)^2$ and the domain of its self-adjoint extension is $H^1(IR^2)^2$. Therefore $-\frac{i}{h}P_0(x,hD)$ generates a strongly continuous group of unitary operators solution to (2.10).

The eigenvalues $\lambda_\pm(x,\xi)=U(x)\pm|\xi|$ of the symbol $P_0(x,\xi)$ satisfy $\lambda_+(x,\xi)=\lambda_-(x,\xi)$ at the crossing set $\{\xi=0\}\subset IR^2_x\times IR^2_\xi$. The semiclassical limit away from the crossing set was performed in [13] for systems of the form (2.10) with more general symbols and initial data u_I^h subject to additional conditions. In [13], the authors show that the semiclassical limit for the different bands can be treated separately where, for each band, the related eigenvalue plays the role of a scalar classical Hamiltonian.

2.1 Adiabatic semiclassical limit

We recall now some basic notions of the Wigner analysis involved in the semiclassical limit. For $u,v\in L^2(IR^2)$, the Wigner transform is defined by:

$$w^h(u,v)(x,\xi)=\frac{1}{(2\pi)^2}\int_{IR^2}u\left(x-h\frac{y}{2}\right)\overline{v}\left(x+h\frac{y}{2}\right)e^{i\xi.y}dy$$

and for $u\in\mathcal{H}$, the 2×2 Wigner matrix is defined by:

$$W^h[u]=\Big(w^h(u_i,u_j)\Big)_{1\le i,j\le 2}.$$

We denote by $w^h[u]=\mathrm{tr}W^h[u]$ the scalar Wigner transform of u. For any bounded sequence f^h in $\mathcal{H}$, there is a subsequence of $W^h[f^h]$ which converges in $\mathcal{S}'$. Such a limit W^0 is called a Wigner measure associated to f^h. If f^h admits only one Wigner measure, we shall denote it by $W^0[f^h]$ and set $w^0[f^h]=\mathrm{tr}W^0[f^h]$.

Another important object is the classical flow $\phi_t^{\pm}(x,\xi)=(x^{\pm}(t),\xi^{\pm}(t))$ corresponding to the eigenvalues $\lambda_{\pm}$, i.e. the solution to:

$$\begin{cases} \frac{d}{dt}x^{\pm}(t)=\pm\frac{\xi^{\pm}(t)}{|\xi^{\pm}(t)|}, & x^{\pm}(0)=x,\\ \frac{d}{dt}\xi^{\pm}(t)=-\partial_x U(x^{\pm}(t)), & \xi^{\pm}(0)=\xi, \end{cases} \tag{2.12}$$

where $(x,\xi)\in IR^2_x\times IR^2_\xi$. Indeed, the decoupled semiclassical limit is valid on a set of the phase space which is stable under the flow $\phi_t^{\pm}$ and where no band crossing occurs. More precisely, if there exists an open subset $\Omega\subset IR^2_x\times IR^2_\xi$ such that:

$$\Omega\cap\{\xi=0\}=\emptyset \quad\text{and}\quad \phi_t^{\pm}(\Omega)\subset\Omega,\ \forall t\in IR$$

and if the initial condition u_I^h in (2.10) has a Wigner measure W_I^0 such that $w_I^0=\mathrm{tr}W_I^0$ satisfies

$$w_I^0|_{\Omega^c}=0,$$

then using the results in [13], it holds that $w^h[u^h]$, the scalar Wigner transform of the solution u^h to (2.10), converges to

$$w^0(t,x,\xi)=w_+^0(t,x,\xi)+w_-^0(t,x,\xi), \tag{2.13}$$

where $w_{\pm}^0(t,\cdot,\cdot)$ is the scalar positive measure on $IR^2_x\times IR^2_\xi$ solving the classical Liouville equations:

$$\begin{cases} \partial_t w_{\pm}^0\pm\frac{\xi}{|\xi|}\partial_x w_{\pm}^0-\partial_x U.\partial_\xi w_{\pm}^0=0, & IR_t\times\Omega,\\ w_{\pm}^0(0,\cdot,\cdot)=\mathrm{tr}\left(\Pi_{\pm}W_I^0\right), & \Omega, \qquad w_{\pm}^0(t,\Omega^c)=0, \quad t\in IR. \end{cases} \tag{2.14}$$

For all $(x,\xi)\in\Omega$, $\Pi_{\pm}(\xi)$ in (2.14) denotes the projection on the eigenspace related to the eigenvalue $\lambda_{\pm}(x,\xi)$. Using formula (2.9), it can be expressed explicitly as follows:

$$\Pi_{\pm}(\xi)=\frac{1}{2}\left(I\pm\frac{1}{|\xi|}B(\xi)\right). \tag{2.15}$$

Moreover, the density $n^h(t,x)=|u^h(t,x)|^2$ converges to

$$n^0(t,x)=\int_{IR^2}w^0(t,x,\xi)d\xi.$$

It follows that for initial data u_I^h such that the bands are separated initially, i.e. the support of w_I^0 does not intersect with the crossing set $\{\xi=0\}$, the measure w^0 is described by w_I^0 if the support of w_I^0 is stable under the characteristics solution to (2.12) (in that case, the characteristics starting from the support of w_I^0 do not reach $\{\xi=0\}$).

2.2 Some case studies

2.2.1 Case $U=0$

In the case of the trivial potential, the solutions to (2.12) are given by:

$$\left(x^{\pm}(t),\xi^{\pm}(t)\right)=\left(x\pm\frac{\xi}{|\xi|}t,\xi\right) \tag{2.16}$$

for $\xi\neq 0$ and we can take $\Omega=IR^2_x\times IR^2_\xi\setminus\{\xi=0\}$. Then the system (2.14) writes:

$$\begin{cases} \partial_t w^0_\pm \pm \frac{\xi}{|\xi|}\partial_x w^0_\pm = 0, \quad IR_t\times\{\xi\neq 0\}, \\ w^0_\pm(0,\cdot,\cdot)=w^0_{I,\pm}, \quad \{\xi\neq 0\}, \qquad\qquad w^0_\pm(t,x,0)=0, \quad t\in IR,\ x\in IR^2, \end{cases} \tag{2.17}$$

where

$$w^0_{I,\pm}=\mathrm{tr}\left(\Pi_\pm W^0_I\right), \quad \xi\neq 0.$$

Using (2.16) in (2.17), we get that:

$$w^0_\pm(t,x,\xi)=w^0_{I,\pm}\left(x\mp\frac{\xi}{|\xi|}t,\xi\right), \quad \xi\neq 0.$$

Therefore, the density $n^h(t,x)=|u^h(t,x)|^2$ converges to

$$n^0(t,x)=\int_{IR^2} w^0_{I,-}\left(x+\frac{\xi}{|\xi|}t,\xi\right)d\xi+\int_{IR^2} w^0_{I,+}\left(x-\frac{\xi}{|\xi|}t,\xi\right)d\xi.$$

In the present case, if the support of the initial scalar Wigner measure w^0_I does not contain the point $\{\xi=0\}$, then no hopping occurs: the bands do not communicate and at any time the measure w^0 is described by the separate evolution of the level characteristics.

2.2.2 Case $U=\alpha x_1$, $\alpha\in IR\setminus\{0\}$

In that case, the solutions to (2.12) are such that:

$$\xi^{\pm}(t)=\xi-(\alpha t,0) \tag{2.18}$$

and we can take $\Omega=IR^2_x\times IR^2_\xi\setminus\{\xi_2=0\}$. Then, system (2.14) becomes:

$$\begin{cases} \partial_t w^0_\pm \pm \frac{\xi}{|\xi|}\partial_x w^0_\pm - \alpha\partial_{\xi_1} w^0_\pm = 0, \quad IR_t\times\{\xi_2\neq 0\}, \\ w^0_\pm(0,\cdot,\cdot)=\mathrm{tr}\left(\Pi_\pm W^0_I\right), \quad \{\xi_2\neq 0\}, \qquad w^0_\pm(t,x,(\xi_1,0))=0, \quad t\in IR,\ x\in IR^2,\ \xi_1\in IR. \end{cases} \tag{2.19}$$

Unlike in Section 2.2.1, non-adiabatic transfer may occur. Indeed, if the support of w^0_I does not intersect with the crossing set $\{\xi=0\}$ but contains points of the form (x,ξ) where $\xi=(\xi_1,0)$ and $\xi_1\neq 0$, then the characteristic curve $\xi^{\pm}(t)$, given by (2.18), starting

from $(\xi_1,0)$, will reach the crossing set at the time $t=\frac{\xi_1}{\alpha}$ and a band-to-band transition will take place.

In these conditions, the system (2.19) does not describe correctly the asymptotics $h\to 0$ of the Wigner matrix $W^h[u^h]$.

The goal of this paper is to develop efficient semiclassical methods to compute the non-adiabatic transition between different bands. To quantify the transition rates, we propose in Section 3 a Landau-Zener formula which can be justified theoretically by using the results in [10]. Indeed, in [10] the following symbol was considered:

$$P_1(x,\xi)=A(\xi)+U(x)I,\quad (x,\xi)\in IR^2_x\times IR^2_\xi, \tag{2.20}$$

where I is the 2×2 identity matrix and

$$A(\xi)=\begin{pmatrix}\xi_1 & \xi_2\\ \xi_2 & -\xi_1\end{pmatrix}. \tag{2.21}$$

Using the unitary equivalence

$$B(\xi)=R^*A(\xi)R, \tag{2.22}$$

where

$$R=\frac{1}{\sqrt{2}}\begin{pmatrix}1 & 1\\ i & -i\end{pmatrix}, \tag{2.23}$$

it follows that the two symbols have the same eigenvalues and P_0 can be reduced to P_1 after conjugation with the matrix R in the treatment of band crossing.

Remark 2.1. The functions $w^0_\pm(t,x,\xi)$ in (2.13) are the diagonal terms of the Wigner measure $W^0(t,x,\xi):=W^0[u^h(t)](x,\xi)$. Indeed, it was shown in [13] that $w^0_\pm$ is given by

$$w^0_\pm=\mathrm{tr}\left(\Pi_\pm W^0\right)1_\Omega \tag{2.24}$$

and that W^0 is diagonal in the sense that $W^0=\Pi_+W^0\Pi_++\Pi_-W^0\Pi_-$ on $IR_t\times\Omega$. Moreover, an easy computation leads to:

$$\Pi_\pm W^0\Pi_\pm=\mathrm{tr}\left(\Pi_\pm W^0\right)\Pi_\pm=w^0_\pm\Pi_\pm\quad \text{on}\quad IR_t\times\Omega. \tag{2.25}$$

3 The Landau-Zener transition

In this section we will study the Landau-Zener transition for the Hamiltonian $P_0(x,hD)$.

3.1 Classical flow around the crossing set

As remarked in Section 2, non-adiabatic transfer happens only when the characteristics reach the crossing set $\{\xi=0\}$. Proposition 3.1 below says that such characteristics will exist as soon as the potential has points $x\in IR^2$ such that $\partial_x U(x)\neq 0$. We refer to [10] for the proof.

Proposition 3.1. Consider $x\in IR^2$ such that $\partial_x U(x)\neq 0$, then there exist two unique curves $s\mapsto(x^{\pm}(s),\xi^{\pm}(s))$ which are continuous in s in a neighborhood of 0 and C^1 for $s\neq 0$ and such that:

$$\begin{cases} \frac{d}{ds}x^{\pm}(s)=\pm\frac{\xi^{\pm}(s)}{|\xi^{\pm}(s)|}, & x^{\pm}(0)=x, \\ \frac{d}{ds}\xi^{\pm}(s)=-\partial_x U(x^{\pm}(s)), & \xi^{\pm}(0)=0. \end{cases} \tag{3.1}$$

To illustrate the fact that a spectral transfer for the symbol P_0 happens at the crossing set, we will come back momentarily to the potential $U=\alpha x_1$ introduced in Section 2.2.2. For such a potential, problem (3.1) writes:

$$\begin{cases} \frac{d}{ds}x^{\pm}(s)=\pm\frac{\xi^{\pm}(s)}{|\xi^{\pm}(s)|}, & x^{\pm}(0)=x, \\ \frac{d}{ds}\xi^{\pm}(s)=-\alpha\begin{pmatrix}1\\0\end{pmatrix}, & \xi^{\pm}(0)=0, \end{cases}$$

and $\forall x\in IR^2$, its unique solution is given by:

$$x^{\pm}(s)=x\mp\mathrm{sgn}(\alpha)\begin{pmatrix}|s|\\0\end{pmatrix},\quad \xi^{\pm}(s)=-\alpha\begin{pmatrix}s\\0\end{pmatrix}.$$

Plugging this solution in the projectors defined in (2.15), we get for $s<0$:

$$\Pi_+(\xi^{\pm}(s))=\frac{1}{2}\begin{pmatrix}1 & \mathrm{sgn}(\alpha)\\ \mathrm{sgn}(\alpha) & 1\end{pmatrix},\quad \Pi_-(\xi^{\pm}(s))=\frac{1}{2}\begin{pmatrix}1 & -\mathrm{sgn}(\alpha)\\ -\mathrm{sgn}(\alpha) & 1\end{pmatrix}$$

and for $s>0$:

$$\Pi_+(\xi^{\pm}(s))=\frac{1}{2}\begin{pmatrix}1 & -\mathrm{sgn}(\alpha)\\ -\mathrm{sgn}(\alpha) & 1\end{pmatrix},\quad \Pi_-(\xi^{\pm}(s))=\frac{1}{2}\begin{pmatrix}1 & \mathrm{sgn}(\alpha)\\ \mathrm{sgn}(\alpha) & 1\end{pmatrix}.$$

It is easy to see that the projectors $\Pi_+(\xi^{\pm}(s))$ and $\Pi_-(\xi^{\pm}(s))$ interchange one with the other when the characteristics pass through the crossing set $\{\xi=0\}$.

3.2 A heuristic derivation of the Landau-Zener formula

In this section, we give a heuristic argument, similar to the one in [24] and [25], to derive the Landau-Zener formula for the Hamiltonian $P_0(x,hD)$.

In general, the region for non-adiabatic transfer is not restricted to the crossing set $\{\xi=0\}$, since quantum transition occurs as long as the two energy levels are sufficiently close, in the case of avoided crossing [15]. As in [24] and [25], we define this region to contain the points where the distance between the eigenvalues $\lambda_{\pm}(x,\xi)$ of $P_0(x,\xi)$ is minimal. In our case $|\lambda_+(x,\xi)-\lambda_-(x,\xi)|=2|\xi|$ and, when considered along the characteristics solution to (2.12), the necessary condition for minimal gap is:

$$\left(|\xi(s)|^2\right)'=0\Leftrightarrow\xi(s).\partial_x U(x(s))=0$$

and the hopping surface is chosen as the set:

$$S=\{(x,\xi)\in IR^4;\xi.\partial_x U(x)=0\}. \tag{3.2}$$

The heuristics follows by inserting the characteristics in the trace-free part of the symbol to obtain the system of ordinary differential equations:

$$ih\psi'(s)=B(\xi(s))\psi(s).$$

After conjugation with the matrix R defined in (2.23) and using equation (2.22), one arrives at the following new system:

$$ih\psi'(s)=A(\xi(s))\psi(s).$$

Assume the particles defined by the trajectory ((2.12)) are near a point $(x^*,\xi^*)\in S$ (due to translation invariance we assume particles are at (x^*,ξ^*) initially), then the Taylor expansion gives:

$$\begin{aligned} x(s)&=x^*\pm\frac{\xi^*}{|\xi^*|}s+\mathcal{O}(s^2),\\ \xi(s)&=\xi^*-\partial_x U(x^*)s+\mathcal{O}(s^2). \end{aligned}$$

Ignoring the $\mathcal{O}(s^2)$ terms, the system becomes:

$$ih\psi'(s)=\begin{pmatrix} \xi_1^*-\partial_{x_1}U(x^*)s & \xi_2^*-\partial_{x_2}U(x^*)s\\ \xi_2^*-\partial_{x_2}U(x^*)s & -\xi_1^*+\partial_{x_1}U(x^*)s \end{pmatrix}\psi(s).$$

After conjugation with the rotation matrix:

$$\begin{pmatrix} \cos\theta & \sin\theta\\ -\sin\theta & \cos\theta \end{pmatrix},$$

where θ is the angle such that

$$(\cos 2\theta,\sin 2\theta)=\frac{\partial_x U(x^*)}{|\partial_x U(x^*)|},$$

we get:

$$i\frac{h}{|\partial_x U(x^*)|}\psi'(s)=\begin{pmatrix} -s & \frac{\xi^*\wedge\partial_x U(x^*)}{|\partial_x U(x^*)|^2}\\ \frac{\xi^*\wedge\partial_x U(x^*)}{|\partial_x U(x^*)|^2} & s \end{pmatrix}\psi(s),$$

where $\xi\wedge\zeta=\xi_2\zeta_1-\xi_1\zeta_2$ for $\xi,\zeta\in IR^2$. After conjugation with the matrix

$$\begin{pmatrix} 0 & 1\\ 1 & 0 \end{pmatrix},$$

it follows:

$$i\frac{h}{|\partial_x U(x^*)|}\psi'(s)=\begin{pmatrix} s & \frac{\xi^*\wedge\partial_x U(x^*)}{|\partial_x U(x^*)|^2} \\ \frac{\xi^*\wedge\partial_x U(x^*)}{|\partial_x U(x^*)|^2} & -s \end{pmatrix}\psi(s).$$

If we set $\varepsilon=\frac{h}{|\partial_x U(x^*)|}$ and $\eta=\frac{\xi^*\wedge\partial_x U(x^*)}{|\partial_x U(x^*)|^2}$, the system becomes:

$$i\varepsilon\psi'(s)=\begin{pmatrix} s & \eta \\ \eta & -s \end{pmatrix}\psi(s),$$

which is the well known Landau-Zener problem (see [40]) for which the transition probability is:

$$T=e^{-\frac{\pi}{\varepsilon}\eta^2}.$$

This allows us to propose the following non-adiabatic transition rate at the point (x^*,ξ^*):

$$T(x^*,\xi^*)=e^{-\frac{\pi}{h}\frac{\left(\xi^*\wedge\partial_x U(x^*)\right)^2}{|\partial_x U(x^*)|^3}}. \tag{3.3}$$

3.3 About the rigorous justification of the Landau-Zener formula

As already noticed in Section 2, the symbol P_0 involved in the Dirac equation (2.10) satisfies the identity

$$P_1(x,\xi)=RP_0(x,\xi)R^*,$$

where P_1 and R are given respectively by (2.20) and (2.23). Therefore, if u^h denotes the solution to (2.10), the function $v^h=Ru^h$ satisfies the equation:

$$ih\partial_t v^h=P_1(x,hD)v^h, \tag{3.4}$$

where $P_1(x,hD)$ is defined as in (2.11). The Landau-Zener formula was obtained rigorously in [10] for the two-scale Wigner measure $\tilde{v}$ of the function v^h (see [10], [25] for the definition of two-scale Wigner measures). This result is shown under precise assumptions, gathered in Assumption 1.2 of [11], on the initial data $v^h|_{t=0}$, its Wigner transform and the potential $U(x)$. It provides a rigorous proof of our Landau-Zener formula. Indeed, if ν_I denotes the two-scale Wigner measure of u^h, it follows that the two-scale Wigner measure of v^h is $\tilde{v}=R\nu_I R^*$. Then, the Landau-Zener formula for ν_I can be deduced from the Landau-Zener formula for $\tilde{v}$.

Remark 3.1. The Landau-Zener formula obtained in [10] writes

$$T=e^{-\frac{\pi\eta^2}{|\partial_x U(x)|}},$$

where

$$\eta=\delta\xi\wedge\frac{\partial_x U}{|\partial_x U|}.$$

When the direction $\delta\xi$ is equal to $\frac{\xi}{\sqrt{h}}$, this corresponds to the Landau-Zener formula (3.3) that we obtained heuristically in Section 3.2.

4 A surface hopping algorithm

We give here a semiclassical Lagrangian algorithm for the evolution of the diagonal terms of the Wigner matrix $W^h(t,x,\xi)$ of the solution $u^h(t)$ to (2.10). The algorithm is adopted from the method proposed in [24] for time-dependent two-level Schrödinger systems with conically intersecting eigenvalues.

Define the level populations:

$$P^h_\pm(t) = ||\Pi_\pm(hD)u^h(t)||^2_{\mathcal{H}}, \tag{4.1}$$

where for $u\in\mathcal{H}$, $\Pi_\pm(hD)u$ is the function defined via its Fourier transform $\Pi_\pm(h\xi)\hat{u}(\xi)$ and $\hat{u}=\mathcal{F}u$ is given by:

$$\mathcal{F}u(\xi) = \frac{1}{2\pi}\int_{IR^2} u(x)e^{-ix.\xi}dx$$

(it is clear from (2.15) that $\Pi_\pm(hD)u=\Pi_\pm(D)u$). With similar computations as in [24], we obtain:

$$P^h_\pm(t) = \int_{IR^2_x}\int_{IR^2_\xi} w^h_\pm(t,x,\xi)dxd\xi, \tag{4.2}$$

where

$$w^h_\pm(t,x,\xi) = \mathrm{tr}\left(\Pi_\pm(\xi)W^h(t,x,\xi)\right). \tag{4.3}$$

As it appears from the following equation

$$\Pi_\pm W^h\Pi_\pm = w^h_\pm\Pi_\pm,$$

which is obtained in a similar way as (2.25), $w^h_\pm$ are the diagonal terms of the Wigner matrix W^h. Up to a small remainder, the function $w^h_\pm$ can be written in terms of the scalar Wigner transform of the level projections of the solution $u^h(t)$. Indeed, using Lemma 2.3 in [13], it holds for all $t\in IR$:

$$w^h_\pm(t) = w^h\left[u^h_\pm(t)\right] + o(1) \tag{4.4}$$

in $\mathcal{D}'\left(IR^2_x\times(IR^2_\xi\setminus\{\xi=0\})\right)$ when $h\to 0$, where $u^h_\pm(t)$ is the function with Fourier transform given by

$$\hat{u}^h_\pm(t,\xi) = \Pi_\pm(h\xi)\hat{u}^h(t,\xi)1_{\xi\neq 0},$$

and $\hat{u}^h(t)$ is the Fourier transform of $u^h(t)$. Comparing the relations (4.3) and (2.24), it follows that, in the situation of Section 2 without band-crossing, the partial differential equation in (2.14) satisfied by $w^0_\pm$ can be used to approximate the time evolution of $w^h_\pm$. In the case of band crossing, the idea is to use (2.14) for the time evolution of $w^h_\pm$ as long as the classical trajectories solution to (2.12) are away from the hopping surface S defined by (3.2). When a trajectory reaches a point $(x^*,\xi^*)\in S$ a non-adiabatic transfer of weight occurs between w^h_+ and w^h_- with transition probability $T(x^*,\xi^*)$ given by (3.3).

The algorithm

1. Initial sampling: in this step, an appropriate sampling of the function $w^h_{I,\pm}$ defined in (4.8) is chosen. Specifically, a set of sampling points

$$\left\{(x_k,\xi_k,j_k)\in IR^2_x\times IR^2_\xi\times\{-,+\};\, k=1,\cdots,N\right\}$$

are chosen with associated weights $w_k\in IR$ given by:

$$w_k=w^h_{I,j_k}(x_k,\xi_k).$$

2. Hopping transport: away from the set S, each particle (x_k,ξ_k,j_k) is transported by the associated classical flow $\phi^{j_k}_t$ solution to (2.12). In other words, for $t\geq 0$ small enough:

$$(x_k(t),\xi_k(t))=\phi^{j_k}_t(x_k(0),\xi_k(0)),\quad w_k(t)=w_k(0). \tag{4.5}$$

If there exists $t^*>0$ such that $(x_k(t^*),\xi_k(t^*))=:(x^*_k,\xi^*_k)\in S$, the weight is reduced using the transition rate

$$T^*=T(x^*_k,\xi^*_k),$$

where $T(x,\xi)$ is given by (3.3). Moreover, in order to describe completely the non-adiabatic transfer, a new particle with index $l>N$ is created. Specifically, for $t>t^*$

$$(x_k(t),\xi_k(t))=\phi^{j_k}_t(x_k(0),\xi_k(0)),\quad w_k(t)=(1-T^*)w_k(t^*)$$

and the new particle is created for $t>t^*$

$$(x_l(t),\xi_l(t))=\phi^{j_l}_{t-t^*}(x^*_k,\xi^*_k),\quad j_l=-j_k,\quad w_l(t)=T^*w_k(t^*).$$

3. Final reconstruction: at the final time $t_f>0$, there are $M\geq N$ points

$$\left\{(x_k,\xi_k,j_k)\in IR^2_x\times IR^2_\xi\times\{-,+\};\, k=1,\cdots,M\right\}$$

with associated weights w_k which are approximations to $w^h_{j_k}(t_f,x_k,\xi_k)$. Then, using Eq. (4.2), the surface hopping approximations $P^h_{sh,\pm}(t_f)$ of the level populations $P^h_\pm(t_f)$ are given by:

$$P^h_{sh,\pm}(t_f)=\sum_{k=1}^{M}w_k\delta^{\pm}_{j_k}\omega_k, \tag{4.6}$$

where δ^i_j is the Kronecker symbol related to i and j, and ω_k is an appropriate quadrature weight.

Remark 4.1. We note that this surface hopping algorithm is subject to some restrictions. First only the dynamics of the diagonal components of the Wigner matrix away from the crossing set are well approximated. Second, there are possible interferences which are not captured if no particular treatment is performed. Indeed, if $w_+^h(t,x,\xi)$ and $w_-^h(t,x,\xi)$ arrive at the same time at some point (x,ξ) close to the crossing set then a transfer of weight using only the Landau-Zener formula (3.3) might give an incorrect approximation of the dynamics. To avoid these interferences, we make the assumption that the initial data u_I^h in (2.10) satisfies

$$\Pi_-(h\xi)\hat{u}_I^h(\xi)=0, \tag{4.7}$$

where $\hat{u}_I^h$ is the Fourier transform of u_I^h. Then, it follows from (4.4) that the diagonal terms of the initial Wigner matrix

$$w_{I,\pm}^h(x,\xi)=\mathrm{tr}\left(\Pi_\pm(\xi)W^h\left[u_I^h\right](x,\xi)\right) \tag{4.8}$$

satisfy in $\mathcal{D}'\left(IR_x^2\times(IR_\xi^2\setminus\{\xi=0\})\right)$

$$w_{I,+}^h=w^h\left[u_I^h\right]+o(1),\quad w_{I,-}^h=o(1) \tag{4.9}$$

when $h\to 0$. Therefore, for the potential $U(x)=\alpha x_1$ given in Section 2.2.2, the condition (4.7) insures that no interferences occur. Indeed, if $w_+^h(t,x,\xi)$ reaches the crossing set $\{\xi=0\}$ at some time $t^*>0$, the particle corresponding to $w_-^h(t,x,\xi)$ immediately moves away as it appears from the equation

$$\xi^\pm(t)=-\alpha(t-t^*,0) \tag{4.10}$$

for the momentum part of the characteristics solution to (2.12). Similarly, in the case where the potential has no stationary points, i.e. $\partial_x U(x)\neq 0$, $\forall x\in IR^2$, Eq. (4.10) is replaced by

$$\xi^\pm(t)=-\int_{t^*}^t \partial_x U\left(x^\pm(s)\right)ds,$$

and the condition (4.7) insures that no interferences occur as long as $|t-t^*|$ is small enough.

Remark 4.2. To deal with this interference, a possible solution might be to use a hybrid method for the Dirac equation (2.10). Such a method was introduced in [22] for the Schrödinger equation and mixes a Gaussian beam method or a Liouville equation in the region where no-interferences occur and a complete quantum solver in the region where the phase information of the wave function is required. In our case, the second region corresponds to the hopping region. Since the region which involves the quantum solver can be chosen very small, a hybrid method allows an adapted treatment of the interferences without increasing dramatically the numerical cost even if the semiclassical parameter

tends to 0. In addition, the resulting algorithm is supposed to work regardless of the conditions in Remark 4.1 on the potential and the initial data. Another possible solution is to keep the off-diagonal entries, which contain information about the non-adiabatic transition in the Wigner transform, and then derive the semiclassical models for the entire Wigner matrix, see [6, 30]. In the next section, we study such a model.

5 Transition rate of an asymptotic model derived in [30]

As it was mentioned, the surface hopping method breaks down where there are interferences. A possible remedy for this is to derive improved models using the Wigner transform for the *entire* Wigner matrix, in which the off-diagonal entries contain non-adiabatic transition information [6, 30]. In this section, we study such a model obtained in [30], and compare the Landau-Zener transition rate of this model with the one we derived in Section 3. To serve our purpose we will only consider the model for the potential studied in Section 2.2.2, $U=\alpha x_1$, $\alpha\in IR\setminus\{0\}$, for which the Wigner matrix does not depend on the variable x_2. It was shown in [30] how this asymptotic model can describe non-adiabatic transfer as a quantum correction of the decoupled system (2.19).

When the Wigner matrix does not depend on the variable x_2, the system (2.19) reads

$$\begin{cases} \partial_t w_\pm^0 \pm \frac{\xi_1}{|\xi|}\partial_{x_1} w_\pm^0 - \alpha\partial_{\xi_1} w_\pm^0 = 0, \quad IR_t\times\{\xi_2\neq 0\}, \\ w_\pm^0(0,\cdot,\cdot) = \mathrm{tr}\left(\Pi_\pm W_I^0\right), \quad \{\xi_2\neq 0\}; \quad w_\pm^0(t,x,(\xi_1,0)) = 0, \quad t\in IR,\ x\in IR^2,\ \xi_1\in IR. \end{cases} \tag{5.1}$$

By taking into account the scaling (2.4)(2.5), the asymptotic model in [30] is the following correction of (5.1):

$$\begin{cases} \partial_t w_\pm \pm \frac{\xi_1}{|\xi|}\partial_{x_1} w_\pm - \alpha\partial_{\xi_1} w_\pm = \pm\alpha\frac{\xi_2}{|\xi|^2}\mathrm{Im}\left(\frac{\xi_1+i\xi_2}{|\xi|}w_i\right), \quad IR_t\times\{\xi_2\neq 0\}, \\ \partial_t w_i - i\Lambda(\xi)w_i - \alpha\partial_{\xi_1} w_i = -i\frac{\alpha}{2}\frac{\xi_2(\xi_1-i\xi_2)}{|\xi|^3}(w_+ - w_-), \end{cases} \tag{5.2}$$

where

$$\Lambda(\xi) = -\frac{2|\xi|}{h} - \frac{\alpha\xi_2}{|\xi|^2}.$$

In the limit $h\to 0$, the function $w_i(t,x,\xi)$ approximates the off-diagonal terms of the Wigner matrix of the solution u^h to (2.10). As it appears from the last equation in (5.2), the function w_i depends on w_+ and w_-. As a consequence, w_i provides a coupling term at the r.h.s. of the first two equations in (5.2).

Using the method of characteristics, w_i can be expressed as an explicit function of the difference $w_+ - w_-$. Inserting this solution in the first two equations in (5.2), the following approximate equations for $w_\pm$, in the limit $h\to 0$, are obtained in [30]:

$$\partial_t w_\pm \pm \frac{\xi_1}{|\xi|}\partial_{x_1} w_\pm - \alpha\partial_{\xi_1} w_\pm = \mp\tau(\xi)(w_+ - w_-), \quad IR_t\times IR_{x_1}\times IR_{\xi_1}, \tag{5.3}$$

where $\xi_2 \neq 0$ can be considered as a small parameter. In the domain

$$\left\{ \xi \in IR^2 \text{ such that } 0 < |\xi_2| \leq \sqrt{\alpha h} \text{ and } |\xi_1| \leq \frac{\alpha h}{|\xi_2|} \right\},$$

the coefficient $\tau(\xi)$ is given by:

$$\tau(\xi) = \frac{\alpha}{2} \frac{\xi_2}{|\xi|^2} \left(\frac{\pi}{2} \text{sgn}(\alpha \xi_2) - \arctan \frac{\xi_1}{\xi_2} \right), \tag{5.4}$$

where $\text{sgn}(x)$ denotes the sign of x. As it will be the case in Section 6.2 for our surface hopping algorithm, the set $\{\xi_1 = 0\}$ is the important region for the hopping. Indeed, the following lemma (proof left to the reader) shows that the set $\{\xi_1 = 0\}$ plays the role of an interface where, in the limit $\xi_2 \to 0$, the solution to (5.3) will have a discontinuity.

Lemma 5.1. *The function $\xi_1 \mapsto \tau(\xi_1, \xi_2)$ tends in $\mathcal{D}'(IR)$ to $|\alpha| \beta \delta_{\xi_1 = 0}$ when $\xi_2 \to 0$, where*

$$\beta = \frac{\pi^2}{4}. \tag{5.5}$$

In the case $\alpha > 0$, we show below that non-adiabatic transfer is possible using the model (5.3) and give the corresponding transmission matrix at the interface. Define $\omega_\pm$ as the set:

$$\omega_\pm = (IR_t \times IR_{x_1} \times IR_{\xi_1}) \cap \{ \pm \xi_1 > 0 \}$$

and consider an initial condition in the upper band and localized at the right of the interface. In other words, the initial conditions for (5.3) are

$$w_\pm(0, \cdot, \cdot) = w_{I,\pm},$$

where $w_{I,-} = 0$ and $w_{I,+}$ is a function in $C_0^\infty(IR_{x_1} \times IR_{\xi_1})$ which is independent of ξ_2 and has support in ω_+. To perform the limit $\xi_2 \to 0$, the following assumptions are required on the solution to (5.3):

*A*1. For all $\xi_2 \neq 0$, $w_\pm \in C^2(IR_t \times IR_{x_1} \times IR_{\xi_1})$.

*A*2. There is a constant C which does not depend on ξ_2 such that:

$$|\partial_{x_1} w_\pm(t, x_1, \xi_1)| \leq C, \quad \forall (t, x_1, \xi_1) \in \omega_+ \cup \omega_-.$$

*A*3. There is a function $w_\pm^0$ which is continuous on ω_+ and ω_- such that $w_\pm$ tends to $w_\pm^0$ when $\xi_2 \to 0$ uniformly on the compact subsets of ω_+ and ω_-.

*A*4. For all $t^* > 0$ and $x_1^* \in IR$, the limit

$$\lim_{\substack{(t,x_1,\xi_1) \to (t^*, x_1^*, 0) \\ (t,x_1,\xi_1) \in \omega_+}} w_\pm^0(t, x_1, \xi_1) \quad \left(\text{resp.} \lim_{\substack{(t,x_1,\xi_1) \to (t^*, x_1^*, 0) \\ (t,x_1,\xi_1) \in \omega_-}} w_\pm^0(t, x_1, \xi_1) \right)$$

exists and is denoted $w_\pm^r(t^*, x_1^*)$ (resp. $w_\pm^l(t^*, x_1^*)$).

The characteristics related to (5.3) are the classical trajectories $\varphi_t^{\pm}(x_I,\xi_I)=(x_1^{\pm}(t),\xi_1^{\pm}(t))$ solution to:

$$\begin{cases} \frac{d}{dt}x_1^{\pm}(t)=\pm\frac{\xi_1^{\pm}(t)}{\sqrt{\xi_1^{\pm}(t)^2+\xi_2^2}}, & x_1^{\pm}(0)=x_I, \\ \frac{d}{dt}\xi_1^{\pm}(t)=-\alpha, & \xi_1^{\pm}(0)=\xi_I. \end{cases} \tag{5.6}$$

Due to the localization of the support of the initial data $w_{I,+}$, only positive initial momenta $\xi_I>0$ have to be considered in (5.6). Therefore, the classical trajectories will reach the interface $\{\xi_1=0\}$ at the time $t^*=\frac{\xi_I}{\alpha}$. Moreover, due to the condition $w_{I,-}=0$, the behavior at the interface is described by the characteristics corresponding to the upper band only. To be more precise, by differentiating the map $s\mapsto w_{\pm}(s,x_1^+(s),\xi_1^+(s))$, one gets by using (5.3):

$$\frac{d}{ds}\begin{pmatrix} w_+(s,x_1^+(s),\xi_1^+(s)) \\ w_-(s,x_1^+(s),\xi_1^+(s)) \end{pmatrix}=-\tau(\xi^+(s))M\begin{pmatrix} w_+(s,x_1^+(s),\xi_1^+(s)) \\ w_-(s,x_1^+(s),\xi_1^+(s)) \end{pmatrix}+F(s), \tag{5.7}$$

where

$$\xi^{\pm}(s)=(\xi_1^{\pm}(s),\xi_2),\quad M=\begin{pmatrix} 1 & -1 \\ -1 & 1 \end{pmatrix}\quad\text{and}\quad F(s)=\frac{2\xi_1^+(s)}{|\xi^+(s)|}\begin{pmatrix} 0 \\ \partial_{x_1}w_-(s,x_1^+(s),\xi_1^+(s)) \end{pmatrix}.$$

Applying the Duhamel formula to (5.7), it follows:

$$\begin{pmatrix} w_+(t,x_1^+(t),\xi_1^+(t)) \\ w_-(t,x_1^+(t),\xi_1^+(t)) \end{pmatrix}=e^{-\int_0^t\tau(\xi^+(s))dsM}\begin{pmatrix} w_{I,+}(x_I,\xi_I) \\ w_{I,-}(x_I,\xi_I) \end{pmatrix}+\int_0^t e^{-\int_s^t\tau(\xi^+(\mu))d\mu M}F(s)ds. \tag{5.8}$$

Using (5.4), a direct computation shows that there is a constant C which does not depend on ξ_2 such that:

$$\forall s,t\in IR,\quad \left|\int_s^t\tau(\xi^{\pm}(\mu))d\mu\right|\le C. \tag{5.9}$$

Moreover it holds

$$\lim_{\xi_2\to 0}\int_0^t\tau(\xi^{\pm}(s))ds=\begin{cases} 0 & \text{if } 0<t<t^*, \\ \beta & \text{if } t>t^*. \end{cases} \tag{5.10}$$

In addition, since the lower band is not occupied initially and most of the band-to-band transfer occurs at the time t^*, it holds:

$$\forall 0<t<t^*,\quad \lim_{\xi_2\to 0}\partial_{x_1}w_-(t,x_1^+(t),\xi_1^+(t))=0. \tag{5.11}$$

In order to simplify the presentation, the proof of (5.11) is postponed until the end of the present discussion. Consider first the case $t<t^*$ in (5.8). Using assumption $A2$ and Eqs. (5.9) and (5.11), the dominated convergence theorem can be applied to the second term at the r.h.s. of Eq. (5.8), which leads to:

$$\int_0^t e^{-\int_s^t\tau(\xi^+(\mu))d\mu M}F(s)ds\underset{\xi_2\to 0}{\longrightarrow}0. \tag{5.12}$$

Combining assumption $A3$ with Eqs. (5.10) and (5.12), one can take the limit $\xi_2 \to 0$ in (5.8) and obtain:

$$\begin{pmatrix} w_+^0(t,x_I+t,\xi_I-\alpha t) \\ w_-^0(t,x_I+t,\xi_I-\alpha t) \end{pmatrix} = \begin{pmatrix} w_{I,+}(x_I,\xi_I) \\ w_{I,-}(x_I,\xi_I) \end{pmatrix}. \tag{5.13}$$

To obtain (5.13), we have used the limit below:

$$\lim_{\xi_2\to 0}(x_1^+(t),\xi_1^+(t)) = \begin{cases} (x_I+t,\xi_I-\alpha t) & \text{if } 0<t<t^*, \\ (x_I+2t^*-t,\xi_I-\alpha t) & \text{if } t>t^*, \end{cases}$$

which follows from the explicit formula of the classical trajectories solution to (5.6). Then, by passing to the limit $t \to t^*$ in (5.13), it follows from assumption $A4$:

$$\begin{pmatrix} w_+^r(t^*,x_1^*) \\ w_-^r(t^*,x_1^*) \end{pmatrix} = \begin{pmatrix} w_{I,+}(x_I,\xi_I) \\ w_{I,-}(x_I,\xi_I) \end{pmatrix}, \tag{5.14}$$

where $x_1^* = x_I + t^*$. The case $t > t^*$ follows the same line with the difference that (5.12) has to be replaced by:

$$\int_0^t e^{-\int_s^t \tau(\xi^+(\mu))d\mu M} F(s)ds = \int_0^{t^*} e^{-\int_s^t \tau(\xi^+(\mu))d\mu M} F(s)ds + \int_{t^*}^t e^{-\int_s^t \tau(\xi^+(\mu))d\mu M} F(s)ds. \tag{5.15}$$

The arguments used to deduce (5.12) can be applied here to show that the first integral at the r.h.s of Eq. (5.15) tends to 0 when $\xi_2 \to 0$. Moreover, using assumption $A2$ and Eq. (5.9), the second integral at the r.h.s of Eq. (5.15) is bounded by the quantity $C(t-t^*)$, which tends to 0 when $t \to t^*$ (here C is a constant which does not depend on ξ_2). Then, by taking successively the limit $\xi_2 \to 0$ and $t \to t^*$ in (5.8), we obtain:

$$\begin{pmatrix} w_+^l(t^*,x_1^*) \\ w_-^l(t^*,x_1^*) \end{pmatrix} = e^{-\beta M} \begin{pmatrix} w_{I,+}(x_I,\xi_I) \\ w_{I,-}(x_I,\xi_I) \end{pmatrix}. \tag{5.16}$$

Putting together (5.14) and (5.16), we get

$$\begin{pmatrix} w_+^l(t^*,x_1^*) \\ w_-^l(t^*,x_1^*) \end{pmatrix} = \begin{pmatrix} 1-T & T \\ T & 1-T \end{pmatrix} \begin{pmatrix} w_+^r(t^*,x_1^*) \\ w_-^r(t^*,x_1^*) \end{pmatrix}, \tag{5.17}$$

where the transition probability T is given by:

$$T = \frac{1-e^{-2\beta}}{2}, \tag{5.18}$$

and the constant β is defined in (5.5). The system (5.17) has the form of the solution of the well known Landau-Zener problem (see [40]). Since x_I and $\xi_I > 0$ are arbitrary, Eq. (5.17) is true for any $t^* > 0$ and $x_1^* \in IR$.

We can now give the proof of (5.11). Differentiating (5.3) with respect to x_1 gives the following PDE for $\partial_{x_1} w_-$:

$$\partial_t(\partial_{x_1} w_-) - \frac{\xi_1}{|\xi|}\partial_{x_1}(\partial_{x_1} w_-) - \alpha\partial_{\xi_1}(\partial_{x_1} w_-) = \tau(\xi)(\partial_{x_1} w_+ - (\partial_{x_1} w_-)). \tag{5.19}$$

Consider $\varphi_s^-(\tilde{x}_I,\xi_I)=(x_1^-(s),\xi_1^-(s))$, the lower band classical trajectory solution to (5.6) with an initial condition $(\tilde{x}_I,\xi_I)$ such that $\varphi_t^-(\tilde{x}_I,\xi_I)=\varphi_t^+(x_I,\xi_I)$. Then it holds

$$\partial_{x_1} w_-(t,x_1^-(t),\xi_1^-(t))=\partial_{x_1} w_-(t,x_1^+(t),\xi_1^+(t)),$$

and it is enough to show that $\partial_{x_1} w_-(t,x_1^-(t),\xi_1^-(t))$ tends to 0 when ξ_2 tends to 0. Now, if one differentiates the map $s\mapsto\partial_{x_1} w_-(s,x_1^-(s),\xi_1^-(s))$, one gets using (5.19):

$$\frac{d}{ds}\left(\partial_{x_1} w_-(s,x_1^-(s),\xi_1^-(s))\right)=\tau(\xi^-(s))\left(\partial_{x_1} w_+(s,x_1^-(s),\xi_1^-(s))-\partial_{x_1} w_-(s,x_1^-(s),\xi_1^-(s))\right).$$

By integrating the previous equation with the Duhamel formula, it follows:

$$\partial_{x_1} w_-(t,x_1^-(t),\xi_1^-(t))=\int_0^t e^{-\int_s^t \tau(\xi^-(\mu))d\mu}\tau(\xi^-(s))\partial_{x_1} w_+(s,x_1^-(s),\xi_1^-(s))ds, \tag{5.20}$$

where we have used that $w_{I,-}=0$. Using assumption $A2$, together with Eqs. (5.9) and (5.10), we can conclude that $\forall 0<t<t^*$, the integral at the r.h.s. of (5.20) tends to 0 when $\xi_2\to 0$.

Remark 5.1. Although the system (5.17) has the correct form, the formula (5.18) for the transition probability is different from the Landau-Zener transition probability (3.3) obtained in Section 3.2 and which writes for our particular potential:

$$T=e^{-\frac{\pi\xi_2^2}{\hbar|\alpha|}}. \tag{5.21}$$

It will be verified numerically in Section 6.4 that the band transmission corresponding to the effective model (5.3) is given by (5.18) whereas the band transmission corresponding to the model (5.2) is given by the correct transition probability (5.21). Therefore, the main finding of the present section is that (5.3) does not agree with the results of the surface hopping algorithm. On the other hand, the results of the surface hopping algorithm agree with those of the original Dirac equation.

Remark 5.2. If the coefficient τ is replaced by $\frac{1}{\xi_2}$, (5.3) becomes a hyperbolic relaxation system (see [19,33]) and the solution to (5.3) satisfies $w_+=w_-$ when $\xi_2\to 0$. Since $\int w_+ + \int w_- = 1$ this leads to:

$$\int w_+ = \int w_- = \frac{1}{2}. \tag{5.22}$$

We will observe numerically in Fig. 11 that (5.22) is true when the time is big enough.

6 Numerical results

In this section, the results provided by the surface hopping algorithm are compared with the reference level populations given by (4.1) where the solution $u^h(t)$ is computed numerically using an accurate method to solve the Dirac equation (2.10). In particular, it

is verified numerically in Section 6.1 that the spectral method is more accurate than the finite difference method. The image of the operator $\Pi_{\pm}(hD)$ is computed by using discrete Fourier transform (DFT) and Fourier multiplication. A comparison of the surface hopping algorithm with the models (5.2) and (5.3) is given in Section 6.4.

6.1 Setup and quantum level simulations

We suppose that the initial data u_I^h is such that its Fourier transform $\hat{u}_I^h$ satisfies the relation:

$$\hat{u}_I^h(\xi) = \hat{f}^h(\xi)\chi_+(h\xi), \tag{6.1}$$

where $\chi_+(\xi)$ is defined in (2.9) and $\hat{f}^h(\xi)$ is the Fourier transform of some function $f^h \in L^2(IR^2)$. Such an initial data satisfies the non-interference condition (4.7). We remark that, like for the level population (4.1), $\chi_+(h\xi)$ can be replaced by $\chi_+(\xi)$ in (6.1).

If f^h is bounded in $L^2(IR^2)$, using Lemma 2.3 in [13] again, we obtain the following approximation for the scalar Wigner transform of u_I^h:

$$w^h\left[u_I^h\right] = W^h\left[f^h\right] + o(1) \tag{6.2}$$

in $\mathcal{D}'\left(IR_x^2 \times (IR_\xi^2 \setminus \{\xi = 0\})\right)$ when $h \to 0$, where $W^h\left[f^h\right] = w^h(f^h, f^h)$. By plugging (6.2) in (4.9), we obtain the following asymptotics for the initial value of the diagonal terms of the Wigner matrix:

$$w_{I,+}^h = W^h\left[f^h\right] + o(1), \quad w_{I,-}^h = o(1) \tag{6.3}$$

in $\mathcal{D}'\left(IR_x^2 \times (IR_\xi^2 \setminus \{\xi = 0\})\right)$ when $h \to 0$. In the present section, the initial upper level function is an h-scaled Gaussian wave packet:

$$f^h(x) = (\pi h)^{-\frac{1}{2}} e^{-\frac{|x-x_0^h|^2}{2h} + i\frac{\xi_0 \cdot (x-x_0^h)}{h}}$$

with center $x_0^h \in IR^2$, momentum $\xi_0 \in IR^2$ and norm $\|f^h\|_{L^2(IR^2)} = 1$. Its h-scaled Fourier transform and its Wigner transform can be computed explicitly. Indeed,

$$\mathcal{F}^h f^h(\xi) = (\pi h)^{-\frac{1}{2}} e^{-\frac{|\xi-\xi_0|^2}{2h} - i\frac{x_0^h \cdot \xi}{h}},$$

where $\forall u \in L^2(IR^2), \mathcal{F}^h u(\xi) = h^{-1}\mathcal{F}u(h^{-1}\xi)$. Moreover,

$$W^h\left[f^h\right](x,\xi) = (\pi h)^{-2} e^{-\frac{|x-x_0^h|^2}{h} - \frac{|\xi-\xi_0|^2}{h}}.$$

In this section, the parameter h is equal to its physical value given by (2.7). The effective mass of the electron is given by

$$m = 0.067 m_e,$$

where m_e is the mass of the electron, the Fermi velocity is taken as $v_F = 10^6 m.s^{-1}$ and, having in mind the simulation of devices of size equal to hundreds of nanometers as

in [16, 30], we will take the reference length equal to $L = 500nm$. Then, the numerical value of the parameter h corresponding to formula (2.7) is:

$$h = 3.4557 \times 10^{-3},$$

which is small enough for the problem to be considered in the semiclassical regime. The simulation domain Ω is equal to

$$\Omega = [-10\sqrt{h}, 10\sqrt{h}] \times [-5\sqrt{h}, 5\sqrt{h}].$$

In the next section, we solve the Dirac equation (2.10) for different choice of the potential U by using the time-splitting spectral method (TSSM) presented in Appendix A.

6.1.1 The Klein tunneling

The potential is equal to $U = v_0 1_{x_1 \geq 0}$ which corresponds to a Klein step. For this potential, we compare the TSSM and the Finite difference time domain method (FDTD) in [16]. The center and the momentum of the initial Gaussian wave packet f^h are chosen as

$$x_0^h = (-5\sqrt{h}, 0), \quad \xi_0 = \frac{1}{2}(1, 0).$$

The height of the Klein step and the simulation time are respectively

$$v_0 = 2|\xi_0| \quad \text{and} \quad t_f = 13\sqrt{h}.$$

For the TSSM, the number of grid points is given by

$$N_1 = 256, \quad N_2 = 128$$

and for the FDTD by

$$N_1 = 1024, \quad N_2 = 512.$$

For the two methods, the number of time steps is fixed as 10^4. For $h = 1$, the convergence of the TSSM is spectral in the space variable and of order 2 in the time variable. The FDTD is of order 2 in both the space and time variables. The space and time discretizations are chosen such that the TSSM method has converged according to Section B. The accuracy of the FDTD is discussed below. We remark anyway that the discretization verifies the stability condition of the FDTD, see [16]:

$$\Delta t \leq \frac{\Delta x_1}{\sqrt{2}},$$

where Δx_1 and Δx_2 are the mesh sizes in the x_1 and x_2 directions respectively.

In the present section and in the following section, the superscript h will be omitted for the solution $u^h(t, x)$ to (2.10) and for the initial condition $u_I^h(x)$. Using the discrete Fourier transform (DFT) (A.5), resp. its inverse, to approximate the Fourier transform,

resp. the inverse Fourier transform, we get the following approximation of the projectors $\Pi_\pm(hD)u(t^n,x_j)$:

$$\Pi_\pm(hD)u_j^n=\frac{1}{N_1N_2}\sum_{k\in\mathcal{K}}\Pi_\pm(h\xi_k)\widehat{(u^n)}_k e^{i\xi_k\cdot(x_j-a)},\quad j\in\mathcal{J},\tag{6.4}$$

where $\widehat{(u^n)}_k$ is the Fourier coefficient defined in (A.5) and the discretization is the same as in Appendix A. Then, using formula (4.1), the approximation $P^h_{dir,\pm}(t^n)$ of the level populations $P^h_\pm(t^n)$ of the Dirac equation is given by:

$$P^h_{dir,\pm}(t^n)=\|\Pi_\pm(hD)u^n\|_2^2,\tag{6.5}$$

where $\Pi_\pm(hD)u_j^n$ is defined by (6.4) and for $u=(u_j)_{j\in\mathcal{J}}$, $u_j\in\mathbb{C}^2$, we have

$$\|u\|_2^2=\sum_{j\in\mathcal{J}}|u_j|^2\Delta x_1\Delta x_2.\tag{6.6}$$

Similarly, the initial condition $u_I(x_j)$ defined by (6.1) is approximated by the formula:

$$(u_I)_j=\frac{2\pi}{(b_1-a_1)(b_2-a_2)}\sum_{k\in\mathcal{K}}\hat{f}^h(\xi_k)\chi_+(h\xi_k)e^{i\xi_k\cdot x_j},\quad j\in\mathcal{J}.$$

We remark that in the previous formula, we used the exact value of the Fourier transform $\hat{f}^h(\xi_k)$ instead of the DFT $\widehat{(f^h)}_k$. The initial data for the TSSM with the parameters described above is represented in Fig. 1. In Fig. 2, we depict the evolution with respect to the time t^n of the level populations $P^h_{dir,\pm}(t^n)$ provided by the TSSM and by the FDTD. The curve with title Upper level, resp. Lower level, refers to the plus sign, resp. minus sign, in (6.5) and the curve with title Total refers to the total population $\|u^n\|_2^2$. Initially, the charge is carried completely by the upper level, then non-adiabatic transfer occurs at time $t=0.28$ and the charge is almost all transferred to the lower level. Moreover, we remark that the TSSM is more accurate than the FDTD. Indeed, the TSSM total population at final time is equal to 1 up to an error smaller than 10^{-10} whereas the FDTD total population at final time is equal to 0.9947. This can be explained by the fact that the first method conserves the total mass (A.8) whereas for the second method the total mass decreases at the hopping time (it was shown in [16] that the quantity conserved by the FDTD is not the mass but a related functional). To reduce this mass loss, the number of spatial points has to be chosen big enough which increases the CPU time of the method. In particular, the CPU times corresponding to the simulations of Fig. 2 are the following: 11644.224s for the FDTD, 441.612s for the TSSM.

We remark in Fig. 3 that the transition occurs when the charge reaches the Klein step which is a classically forbidden region for the Upper level. The band transition to the Lower level makes the Klein step an allowed region for the particles, which can tunnel in the region $x_1\geq 0$ with a probability almost equal to 1. This is the Klein paradox, see [37].

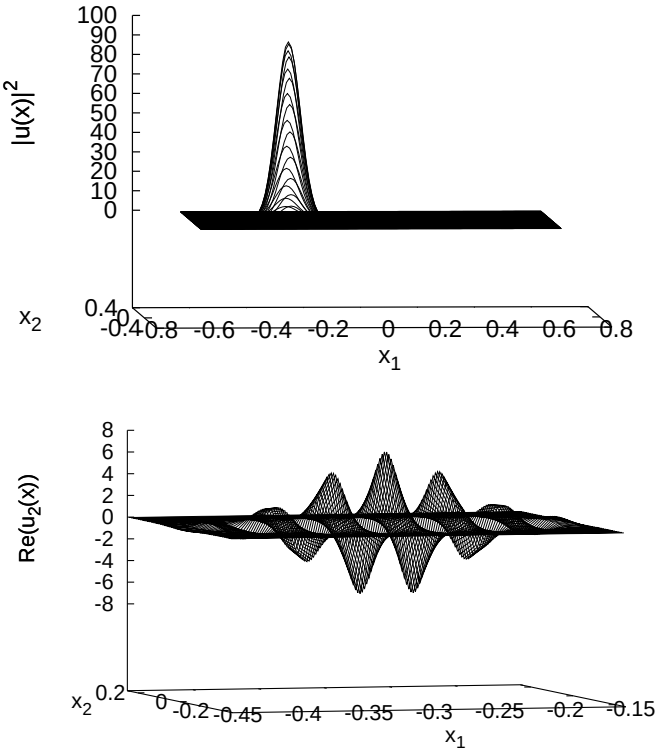

Figure 1: Initial condition for the TSSM: $|u_I(x)|^2$ (top) and, in a smaller region, $\mathrm{Re}((u_I)_2(x))$ (bottom).

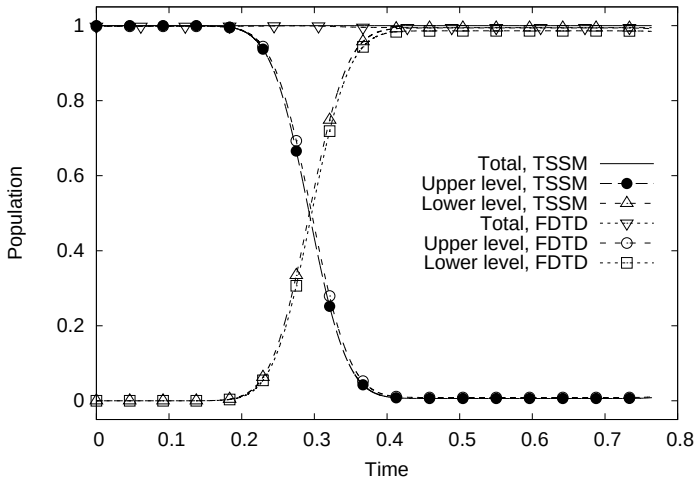

Figure 2: Time evolution of the level populations with a Klein step potential: comparison of the TSSM and the FDTD.

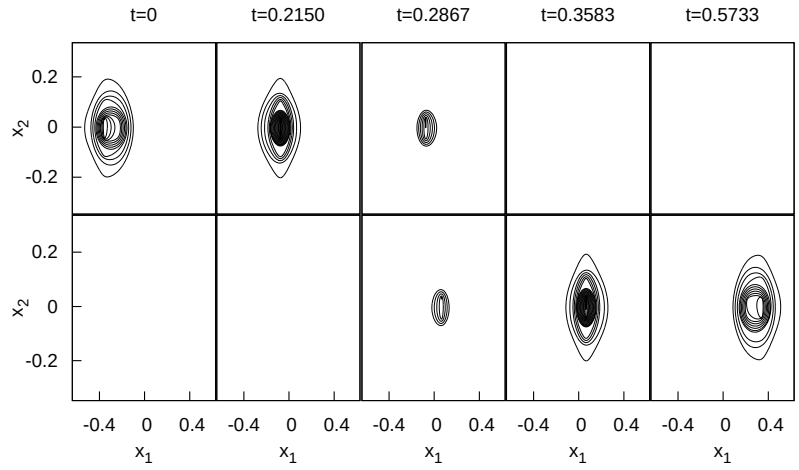

Figure 3: For different times and with respect to the space variable: representation of the position density of the projection of the wave function u solution to (2.10) where $U=v_0 1_{x_1\geq 0}$ and the initial condition is given by (6.1). The upper half corresponds to $|\Pi_+(hD)u_j^n|^2$ and the lower half to $|\Pi_-(hD)u_j^n|^2$ where the projectors are computed using (6.4). The solution u is computed with the TSSM.

6.1.2 Case $U=\alpha x_1$, $\alpha>0$

In this section, the potential is given by $U=\alpha x_1$, $\alpha>0$. The Dirac equation (2.10) is solved using the TSSM. The center and the momentum of the initial Gaussian wave packet f^h are taken to be

$$x_0^h=(-5\sqrt{h},0),\quad \xi_0=(1,0).$$

The level position density of the solution $u^h(t,x)$ to (2.10) is supported around $(x^\pm(t),\xi^\pm(t))$, solution to:

$$\begin{cases} \frac{d}{dt}x^\pm(t)=\pm\frac{\xi^\pm(t)}{|\xi^\pm(t)|}, & x^\pm(0)=x_0^h,\\ \frac{d}{dt}\xi^\pm(t)=-\alpha(1,0), & \xi^\pm(0)=\xi_0. \end{cases}$$

The solution of the above problem can be computed explicitly. It is given by:

$$x^\pm(t)=x^*\mp(|t-t^*|,0),\quad \xi^\pm(t)=\xi_0-\alpha(t,0), \tag{6.7}$$

where $t^*=\frac{(\xi_0)_1}{\alpha}$ is the time such that $\xi^+(t^*)=0$ and the non-adiabatic transfer occurs. The point $x^*=x^+(t^*)=x_0^h+(t^*,0)$ is the point where the hopping occurs. The coefficient α is chosen such that the potential at the hopping point is equal to $U(x^*)=v_0$ where $v_0=\frac{|\xi_0|}{4}$. This leads to:

$$\alpha=\frac{v_0-(\xi_0)_1}{(x_0^h)_1}.$$

The simulation stops at time:

$$t_f=13\sqrt{h}$$

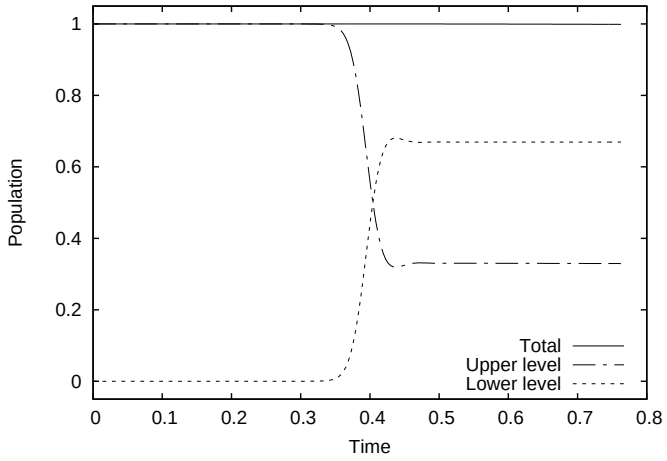

Figure 4: Time evolution of the level populations for the potential $U=\alpha x_1$, $\alpha>0$.

and the number of space points is given by

$$N_1=256, \quad N_2=128.$$

The number of time steps is equal to 10^4. The initial data $(u_I)_j$, the Lower level and Upper level populations $P^h_{dir,\pm}(t^n)$ and the Total population are computed as explained in Section 6.1.1. The time evolution of the level populations is represented in Fig. 4. The numerical hopping is observed around the time $t=0.39$ which is accurate enough compared to the predicted value $t^*=0.3919$ given by (6.7). Contrary to the case of the Klein step potential, a significant part of the charge stays on the upper level.

The predicted value of the position corresponding to the hopping is $x^*=(9.7976\times 10^{-2},0)$. We remark in Fig. 5 that the transition occurs when the charge reaches x^*. As for the Klein step potential, the band transition to the lower level allows the particles to tunnel in the region $x_1\geq x_1^*$. However, for the potential considered here, we can observe that the part remaining on the upper level is reflected. This could have been predicted from Eq. (6.7). Indeed, for $t\geq t^*$, the classical flow corresponding to the upper level (plus sign) moves to the left with respect to x^* whereas the classical flow corresponding to the lower level (minus sign) moves to the right with respect to x^*.

6.2 The surface hopping algorithm

In the present section, the potential U is equal to $U=\alpha x_1$ where $\alpha=15$. The initial condition is as described in Section 6.1. The center and the momentum of the initial Gaussian wave packet f^h are taken as

$$x_0^h=(-5\sqrt{h},0), \quad \xi_0=(1,0). \tag{6.8}$$

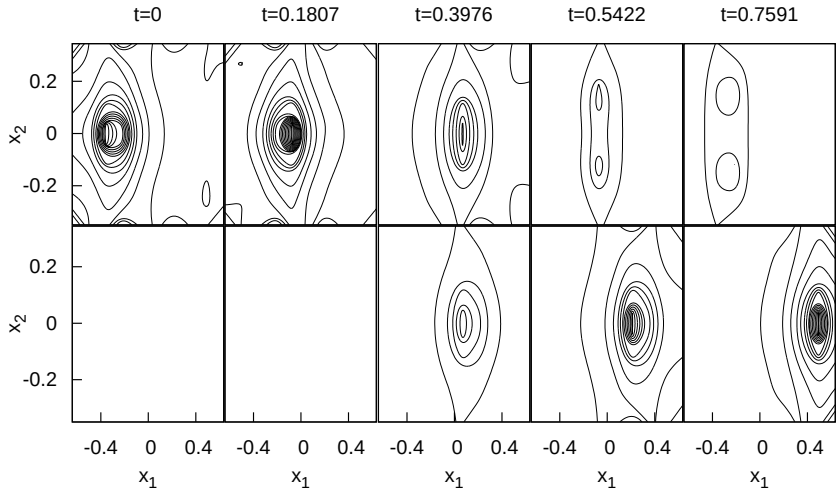

Figure 5: For different times and with respect to the space variable: representation of the position density of the projection of the wave function u solution to (2.10) where $U=\alpha x_1$ and the initial condition is given by (6.1). The upper half corresponds to $|\Pi_+(hD)u_j^n|^2$ and the lower half to $|\Pi_-(hD)u_j^n|^2$ where the projectors are computed using (6.4). The solution u is computed with the TSSM.

The diagonal terms $w_\pm^h(t,x,\xi)$ of the Wigner matrix defined by (4.3) are computed using the surface hopping algorithm presented in Section 4. Then, for different values of the parameter h and of the simulation time t_f, the surface hopping level populations $P_{sh,\pm}^h(t_f)$ are computed from $w_\pm^h(t_f,\cdot,\cdot)$ by using (4.6). The results provided by the surface hopping algorithm are compared to the level populations $P_{dir,\pm}^h(t_f)$ of the Dirac equation computed as explained in Section 6.1.1.

For the level populations $P_{dir,\pm}^h(t_f)$, the Dirac equation (2.10) is solved using the TSSM in the simulation domain

$$\Omega=[-11\sqrt{h},11\sqrt{h}]\times[-5\sqrt{h},5\sqrt{h}].$$

Using Eq. (A.8), we can choose a time step size which does not depend on h. In all the tests, the number of time steps is fixed as 10^4. The number of space points is given by:

$$N_1=256,\quad N_2=128,$$

except for $h=10^{-4}$ where

$$N_1=1024,\quad N_2=512.$$

We verified in Appendix B that, for such a discretization and for all the values of h considered in the present section, the TSSM is accurate enough for the validation of the surface hopping algorithm.

For the level populations $P^h_{sh,\pm}(t_f)$, the initial sampling is chosen as follows. We consider a uniform $J\times J$ discretization of the domain of the x variable:

$$[a_1,b_1]\times[a_2,b_2],$$

where $(a_1,a_2)=x_0^h-5\sqrt{h}$ and $(b_1,b_2)=x_0^h+5\sqrt{h}$ and a uniform $K\times K$ discretization of the ξ variable domain

$$[c_1,d_1]\times[c_2,d_2],$$

where $(c_1,c_2)=\xi_0-5\sqrt{h}$ and $(d_1,d_2)=\xi_0+5\sqrt{h}$. The grid points x_j, $j=1,\cdots,J^2$ and ξ_k, $k=1,\cdots,K^2$ are ordered such that

$$|f^h(x_1)|^2\geq\cdots\geq|f^h(x_{J^2})|^2,$$
$$|\mathcal{F}^h f^h(\xi_1)|^2\geq\cdots\geq|\mathcal{F}^h f^h(\xi_{K^2})|^2.$$

Then, we determine the minimal numbers N_x of points of the x variable and N_ξ of the ξ variable such that

$$\sum_{j=1}^{N_x}|f^h(x_j)|^2\Delta x^2\geq 1-\mathrm{tol}_x,\quad \sum_{k=1}^{N_\xi}|\mathcal{F}^h f^h(\xi_k)|^2\Delta\xi^2\geq 1-\mathrm{tol}_\xi,$$

where $\Delta x=\frac{b_1-a_1}{J}=\frac{b_2-a_2}{J}$, $\Delta\xi=\frac{d_1-c_1}{K}=\frac{d_2-c_2}{K}$ and tol_x, tol_ξ are well chosen tolerances. The phase space points (x_j,ξ_k), $j=1,\cdots,N_x$, $k=1,\cdots,N_\xi$ are ordered such that:

$$W^h\left[f^h\right](x_1,\xi_1)\geq\cdots\geq W^h\left[f^h\right](x_{N_xN_\xi},\xi_{N_xN_\xi}),$$

and we determine the minimal integer N such that:

$$\sum_{k=1}^{N}W^h\left[f^h\right](x_k,\xi_k)\Delta x^2\Delta\xi^2\geq 1-\mathrm{tol},$$

where tol is a well chosen tolerance. This gives the first step of the algorithm of Section 4. Indeed, the initial sampling is the set:

$$\left\{(x_k,\xi_k,+)\in IR^2_x\times IR^2_\xi\times\{-,+\};\ k=1,\cdots,N\right\},$$

where, using Eq. (6.3), the associated weights $w_k\in IR$ can be approximated by:

$$w_k=W^h\left[f^h\right](x_k,\xi_k).$$

In the present case, the hopping surface S defined by (3.2) is equal to:

$$S=\left\{(x,\xi)\in IR^4;\ \xi_1=0\right\},$$

and the second order derivative of the function $s\mapsto|\xi^{\pm}(s)|^2$, defined by the characteristics solution to (2.12), is equal to:

$$\left(|\xi^{\pm}(s)|^2\right)''=2\alpha^2>0.$$

Therefore, for the potential considered here, the points of extremal gap are all minimas.

Moreover, the classical flow $(x^{\pm}(t),\xi^{\pm}(t))$ solution to (2.12) is given by

$$x^{\pm}(t)=x\pm\int_0^t\frac{\xi^{\pm}(s)}{|\xi^{\pm}(s)|}ds,\quad \xi^{\pm}(t)=\xi-\alpha t(1,0). \tag{6.9}$$

In Eq. (6.9), the formula of the momentum is explicit and the hopping transport step can be simplified. Indeed, for $k=1,\cdots,N$, if $0<\frac{(\xi_k)_1}{\alpha}<t_f$, the trajectory $(x_k(t),\xi_k(t))$, $0<t<t_f$ defined by (4.5) will pass through a point $(x_k^*,\xi_k^*)\in S$ at the time $t^*=\frac{(\xi_k)_1}{\alpha}$ and non-adiabatic transfer occurs. For such a k, the weight is changed such that for $t>t^*$

$$w_k(t)=(1-T^*)w_k(t^*),$$

and a new particle is created on the lower band with index $l>N$. For the new particle, the associated weight is such that for $t>t^*$

$$w_l(t)=T^*w_k(t^*).$$

In the above equations, the transition rate T^* is equal to

$$T^*=T(x_k^*,\xi_k^*),$$

where $T(x,\xi)$ is given by (5.21). The surface hopping level populations defined by (4.6) are then given by:

$$P^h_{sh,+}(t_f)=\sum_{k=1}^{N}w_k(t_f)\Delta x^2\Delta\xi^2,\quad P^h_{sh,-}(t_f)=\sum_{l=N+1}^{M}w_l(t_f)\Delta x^2\Delta\xi^2.$$

For all the tests, the size of the sampling grids are equal to:

$$J=K=16.$$

The sampling tolerances are taken as:

$$\text{tol}=10^{-6},\quad \text{tol}_x=\text{tol}_\xi=10^{-3}\times\text{tol}.$$

For such parameters, the number of particles obtained numerically for the initial sampling does not depend on h and is equal to $N=6981$.

For different values of the semiclassical parameter h, the level populations obtained by the two methods are listed in Table 1. The simulation time is fixed as $t_f=0.13$, except for $h=10^{-4}$ where $t_f=0.1$. We remark that the reference lower level population $P^h_{dir,-}(t_f)$

Table 1: At time t_f and for different values of the semiclassical parameter h: level populations obtained by the Dirac solver and the surface hopping method.

h	$P^h_{dir,+}(t_f)$	$P^h_{sh,+}(t_f)$	$P^h_{dir,-}(t_f)$	$P^h_{sh,-}(t_f)$	CPU dir (s)	CPU sh (s)
10^{-1}	7.4804×10^{-2}	9.0741×10^{-2}	0.925196	0.909258	437.284	4.163
10^{-2}	8.9815×10^{-2}	9.0698×10^{-2}	0.910185	0.909301	438.152	4.172
10^{-3}	9.0700×10^{-2}	9.0698×10^{-2}	0.909300	0.909301	434.484	4.160
10^{-4}	9.0698×10^{-2}	9.0698×10^{-2}	0.909301	0.909301	13046.8	4.144

increases when h increases. This is due to the fact that for larger values of h, the transition process is slower and, at the time t_f, the post-transition relaxation observed in Fig. 7, has no yet happened. We notice that, for h smaller or equal to 10^{-2}, the surface hopping level populations $P^h_{sh,\pm}(t_f)$ are almost constant with respect to h. This can be explained by the fact that, for the potential considered, the transition rate depends only on the variable $\xi_2/\sqrt{h}$ which does not depend on h when considered on the sampling points. The column CPU dir, resp. CPU sh, denotes the CPU time required by the Dirac solver, resp. the surface hopping method, to complete the simulations. For the surface hopping algorithm, most of the CPU time corresponds to the choice of the initial sampling (the time effectively spent by the processor on the surface hopping algorithm is smaller than $0.14s$). We remark that the surface hopping CPU times (pre-processing and effective time) are almost h-independent. It appears that the surface hopping method is very interesting. Indeed, when h decreases, the numerical cost of the Dirac solver increases whereas the surface hopping method provides very accurate results for a much smaller CPU time.

We depict in Fig. 6 the absolute error of the level population corresponding to the upper level:

$$\mathcal{E}^h_+(t_f) := |P^h_{dir,+}(t_f) - P^h_{sh,+}(t_f)|, \tag{6.10}$$

with respect to the semiclassical parameter h. The surface hopping level populations converge numerically when $h\to0$ to the level populations obtained at the quantum level. We notice that the convergence order at $h=10^{-4}$ can be improved by proceeding as proposed in Remark B.1.

For $h=10^{-3}$, the time evolution of the level populations provided by the Dirac solver and the surface hopping algorithm are depicted in Fig. 7. The curve with title Upper level dir, resp. Lower level dir, refers to $P^h_{dir,+}(t)$, resp. $P^h_{dir,-}(t)$. The same is true when dir is replaced by sh. The total population of the Dirac equation, curve titled Total dir, is obtained as explained in Section 6.1.1 and the surface hopping total population, curve titled Total sh, corresponds to $P^h_{sh,+}(t)+P^h_{sh,-}(t)$. We observe that the numerically obtained surface hopping total population is conserved. For a smaller CPU time, the time evolution of the level populations provided by the surface hopping algorithm agrees well with the one provided by the Dirac solver. Indeed, for the two methods, the charge is initially carried completely by the upper level, then non-adiabatic transfer occurs at time $t=\frac{(\xi_0)_1}{\alpha}=\frac{1}{15}=0.0667$ (time required by the classical flow to reach the crossing set

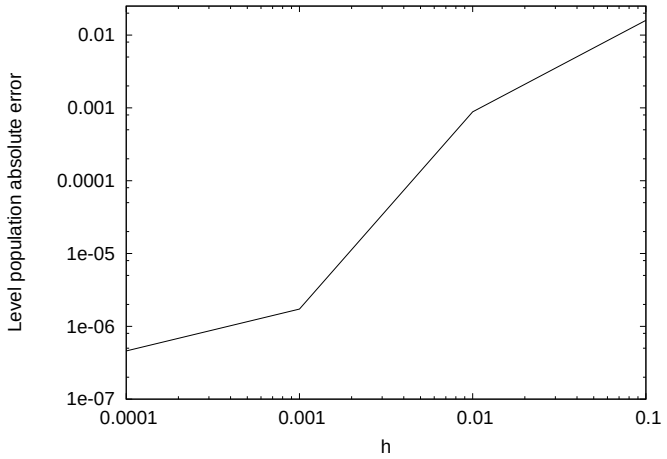

Figure 6: At time t_f, logarithmic plot of the absolute error (6.10) of the level population corresponding to the upper level while varying the semiclassical parameter $h=10^{-p}$, $p=1,2,3,4$.

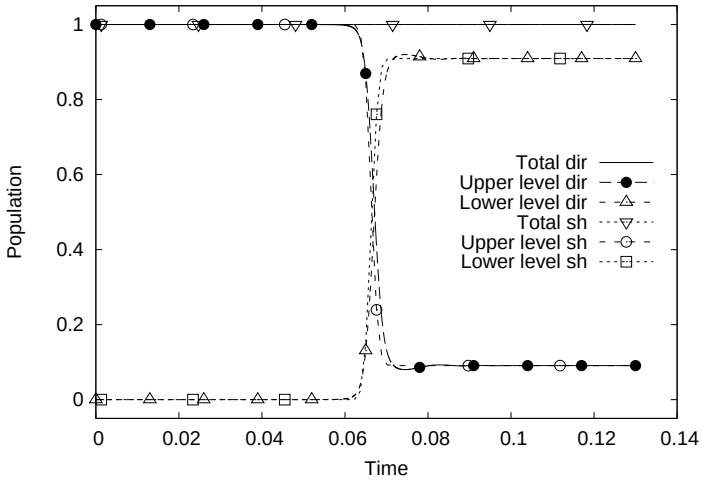

Figure 7: For $h=10^{-3}$ and $U=\alpha x_1$, $\alpha=15$: time evolution of the level populations provided by the Dirac solver and the surface hopping algorithm.

$\{\xi=0\}$ starting from the momentum ξ_0 of the initial Gaussian wave packet) and the great majority of the charge is transferred to the lower level. The CPU time required to complete the simulation is $434.484s$ for the Dirac solver and $9.66400s$ for the surface hopping method. For the second method, the CPU time is bigger than the time indicated in Table 1. This is due to the fact that the surface hopping curves in Fig. 7 are obtained by repeating the surface hopping algorithm described in the present section for the sequence of times $t_f=0.13n/100$, $1\leq n\leq 100$ (the pre-processing step to create the initial sampling is performed only one time).

6.3 Collision of two wave packets

In the present section, the potential is given by $U=\alpha x_1$, $\alpha>0$ and we study the possibility of the interaction of two wave packets, each packet is carried by a different energy level, arriving at the same time at the same point of the hopping surface. In such a situation two non-adiabatic transfers occur at the same time, one from the upper level to the lower level and one from the lower level to the upper level, and we expect that in such a situation the Landau-Zener formula for the transition probability will be affected by interference. It is worth noting that such a breakdown of the semiclassical dynamics due to interference was already observed in [1] in the case of the linear Schrödinger equation with non-smooth potentials.

We suppose that the initial data u_I^h is such that its Fourier transform $\hat{u}_I^h$ satisfies the relation:

$$\hat{u}_I^h(\xi)=\sqrt{\rho}\hat{f}_+^h(\xi)\chi_+(h\xi)+\sqrt{1-\rho}e^{2i\pi\mu}\hat{f}_-^h(\xi)\chi_-(h\xi), \tag{6.11}$$

where $0\leq\rho\leq1$, $0\leq\mu<1$, $\chi_\pm(\xi)$ is defined in (2.9) and $\hat{f}_\pm^h(\xi)$ denotes the Fourier transform of the h-scaled Gaussian wave packet:

$$f_\pm^h(x)=(\pi h)^{-\frac{1}{2}}e^{-\frac{|x-x_{0,\pm}^h|^2}{2h}+i\frac{\xi_0\cdot(x-x_{0,\pm}^h)}{h}},$$

with center $x_{0,\pm}^h\in IR^2$, momentum $\xi_0\in IR^2$ and norm $\|f_\pm^h\|_{L^2(IR^2)}=1$. Such an initial data does not satisfy the non-interference condition (4.7). Using the orthogonality of the eigenvectors $\chi_\pm(\xi)$ and using the same arguments as in Section 6.1, we obtain that the initial level probability densities, populations and diagonal terms of the Wigner matrix are given by:

$$\begin{aligned}
&\widehat{\Pi_+(hD)u_I^h}=\sqrt{\rho}\hat{f}_+^h(\xi)\chi_+(h\xi),\quad \widehat{\Pi_-(hD)u_I^h}=\sqrt{1-\rho}e^{2i\pi\mu}\hat{f}_-^h(\xi)\chi_-(h\xi),\\
&||\Pi_+(hD)u_I^h||_{\mathcal{H}}^2=\rho,\quad ||\Pi_-(hD)u_I^h||_{\mathcal{H}}^2=1-\rho,\\
&w_{I,+}^h=W^h\left[f_+^h\right]+o(1),\quad w_{I,-}^h=W^h\left[f_-^h\right]+o(1),
\end{aligned}$$

where the last relation holds in $\mathcal{D}'\left(IR_x^2\times(IR_\xi^2\backslash\{\xi=0\})\right)$ when $h\to0$. In particular, it holds $\|u_I^h\|_{\mathcal{H}}=1$. The parameter ρ gives the percentage of mass carried by each energy level and the parameter μ is the phase difference between the two wave packets.

For such an initial condition, the position density of the solution $u^h(t,x)$ to (2.10) is composed of two wave packets: one supported around $(x^+(t),\xi^+(t))$ and the other around $(x^-(t),\xi^-(t))$, where $(x^\pm(t),\xi^\pm(t))$ are the characteristics solution to:

$$\begin{cases}
\frac{d}{dt}x^\pm(t)=\pm\frac{\xi^\pm(t)}{|\xi^\pm(t)|}, & x^\pm(0)=x_{0,\pm}^h,\\
\frac{d}{dt}\xi^\pm(t)=-\alpha(1,0), & \xi^\pm(0)=\xi_0.
\end{cases}$$

In the present section, we may have $(\xi_0)_2\neq0$ and (6.7) has to be replaced by:

$$x^\pm(t)=x^{*,\pm}\pm\int_{t^*}^t\frac{\xi^\pm(s)}{|\xi^\pm(s)|}ds,\quad \xi^\pm(t)=\xi^*-\alpha(t-t^*,0),$$

where $t^*=\frac{(\xi_0)_1}{\alpha}$ is the time required to reach the hopping surface (i.e. the time such that $\xi^{\pm}(t^*)=0$) and $(x^{*,\pm},\xi^*)=(x^{\pm}(t^*),\xi^{\pm}(t^*))$ is the point of the phase space where the hopping occurs. The last is given by:

$$x^{*,\pm}=x^h_{0,\pm}\pm\int_0^{t^*}\frac{\xi^{\pm}(s)}{|\xi^{\pm}(s)|}ds,\quad \xi^*=\xi_0-\alpha(t^*,0).$$

To make the interference possible, the two wave packets should not only arrive at the same time at the hopping surface but also at the same point of the phase space, in other words:

$$(x^{*,+},\xi^*)=(x^{*,-},\xi^*). \tag{6.12}$$

If the last equality is not true for the centers of the two wave packet, it should happen at least for characteristics starting from two points of the phase space where the initial probability density is not too small. We remark also that, if $x^h_{0,+}<x^h_{0,-}$, the position characteristics $x^+(t)$ and $x^-(t)$ will get closer from each other when $t<t^*$ and go in opposite directions when $t>t^*$. In that case, when α is fixed, $(\xi_0)_1$ should be chosen so that t^* is big enough to ensure (6.12).

In the present section, we fixed $\alpha=15$ and $h=10^{-3}$. The centers of the initial Gaussian wave packets $f^h_{\pm}$ are taken as:

$$x^h_{0,\pm}=(\mp4\sqrt{h},0).$$

Different simulations will be performed corresponding to the following values of the momentum of the initial Gaussian wave packets $f^h_{\pm}$:

$$\xi_0=(2,0)\quad\text{ and }\quad\xi_0=(2,0.25).$$

The simulation time is fixed as $t_f=0.26$. For the parameters considered here the hopping time is equal to $t^*=0.1333$.

The Dirac level populations $P^h_{dir,\pm}(t)$ are computed as explained in Section 6.2. For $\xi_0=(2,0)$, the simulation domain and the number of space points for the TSSM are given by:

$$\begin{aligned}&\Omega=[-11\sqrt{h},11\sqrt{h}]\times[-5\sqrt{h},5\sqrt{h}],\\&N_1=512,\quad N_2=256.\end{aligned}$$

For $\xi_0=(2,0.25)$, they are given by:

$$\begin{aligned}&\Omega=[-11\sqrt{h},11\sqrt{h}]\times[-10\sqrt{h},10\sqrt{h}],\\&N_1=512,\quad N_2=512.\end{aligned}$$

The number of time steps is fixed as 2×10^4.

The surface hopping algorithm is performed by applying two times the process explained in Section 6.2: one time for each energy level. For the upper level population

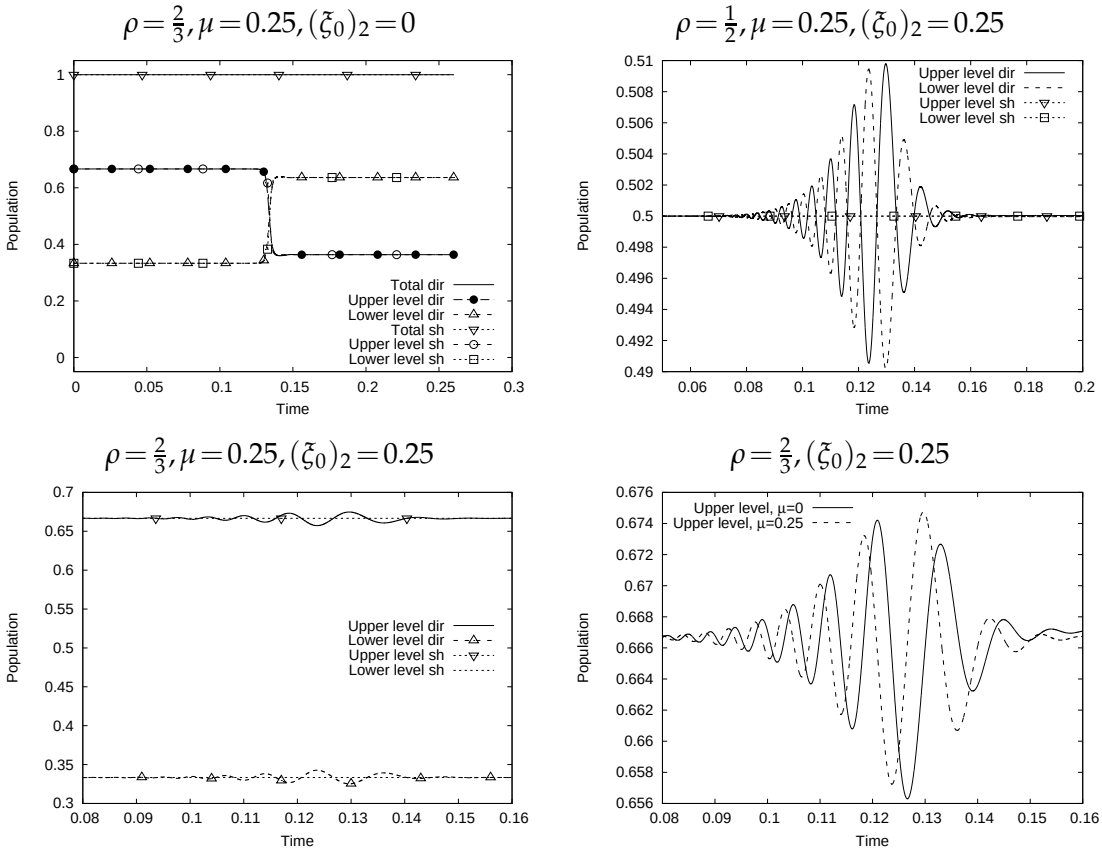

Figure 8: For different values of the parameters ρ, μ and $(\xi_0)_2$: time evolution of the level populations provided by the Dirac solver and the surface hopping algorithm.

$P^h_{sh,+}(t)$ (resp. lower level population $P^h_{sh,-}(t)$), the space domain for the initial sampling is centered at $x^h_{0,+}$ (resp. $x^h_{0,-}$). For each energy level, the size of the sampling grids and the sampling tolerances are the same as in Section 6.2. The number of time steps is fixed as 200.

The time evolution of the level populations provided by the Dirac solver and the surface hopping algorithm for different values of the parameters ρ, μ and $(\xi_0)_2$ are depicted in Fig. 8. The curve with title Upper level dir, resp. Lower level dir, refers to $P^h_{dir,+}(t)$, resp. $P^h_{dir,-}(t)$. The same is true when dir is replaced by sh. In the first graph (top left), we remark that, when the incidence is normal with respect to the line $x_1=(x^{*,\pm})_1$, the two non-adiabatic transfers occur simultaneously without interacting with each other. The second and the third graphs (top right and bottom left) are two situations of incidence with a positive angle with respect to the x_1-axis. In that case there is an interaction between the two levels which is responsible for periodic oscillations of the electrons from the upper energy level to the lower energy level: we will call beating effect such oscil-

lations (a numerical and mathematical analysis of the beating effect in the case of the Schrödinger equation with a double well potential can be found in [3, 14]). As it appears in these graphs, the beating effect is not recovered by the surface hopping algorithm. This shows that the Landau-Zener formula is not valid in the case of interference as expected in Remark 4.1. The last graphic is computed with the Dirac solver and shows that the phase difference between the two initial wave packets implies a translation in the beating oscillations.

In Table 2, we give, for the tests considered in Fig. 8, the absolute error of the level population corresponding to the upper level at the final time t_f. As in Section 6.2, it is given by the formula (6.10). We remark that the oscillations observed in Fig. 8 are localized in a small time interval around the hopping time t^*. After such a time, the surface hopping level populations align again with the quantum ones. For this reason, the absolute errors in Table 2 are all small even when interference occur (there is however an increase of this error in the case of interference: line 2 to 4 of the table).

Table 2: At time t_f and for different values of the parameters ρ, μ and $(\xi_0)_2$: absolute error of the level population corresponding to the upper level.

ρ	μ	$(\xi_0)_2$	Absolute error
2/3	0.25	0	4.8393×10^{-7}
0.5	0.25	0.25	3.5001×10^{-5}
2/3	0.25	0.25	3.3183×10^{-5}
2/3	0	0.25	4.2626×10^{-4}

Fig. 9 corresponds to the second graphic of Fig. 8. It illustrates the fact that the wave packet carried by the upper level and the wave packet carried by the lower level effectively meet in some region of the space variable. The time for this collision matches with the hopping time t^* where both the ξ^+ and ξ^- characteristics starting from ξ_0 reach the hopping surface $\xi_1=0$. As mentioned above, this condition is necessary to have interference in the hopping process.

6.4 Simulations using the models of [30]

In this section we will compare numerically the models (5.2) and (5.3) with the two dimensional version of our surface hopping algorithm. The comparison will be performed with $h=10^{-3}$, $t_f=0.13$ and with the same potential as is Section 6.2. The initial condition is the 2D version of the initial condition in Section 6.2. In other words:

$$w_+^h|_{t=0}=W^h[f^h],\quad w_-^h|_{t=0}=0$$

is replaced by

$$w_+(0,x_1,\xi_1)=(\pi h)^{-1}e^{-\frac{(x_1-(x_0^h)_1)^2}{h}-\frac{(\xi_1-(\xi_0)_1)^2}{h}},\quad w_-(0,x_1,\xi_1)=0. \tag{6.13}$$

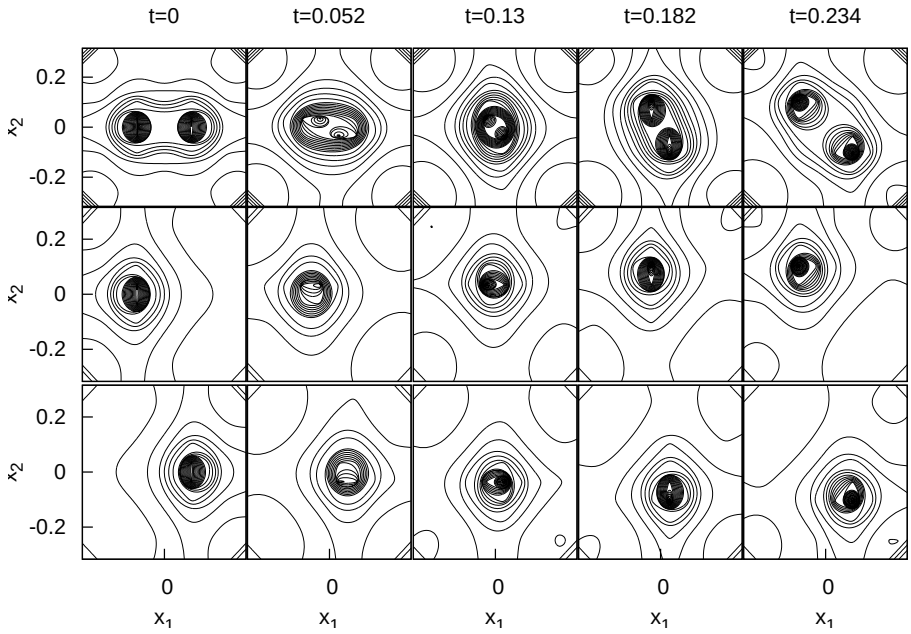

Figure 9: For different times and with respect to the space variable: representation of the position density of the wave function u solution to (2.10) and of its projection where the initial condition is given by (6.11). The first line corresponds to $|u_j^n|^2$, the second line to $|\Pi_+(hD)u_j^n|^2$ and the third line to $|\Pi_-(hD)u_j^n|^2$. The solution u is computed with the TSSM and the parameters $\rho=\frac{1}{2},\mu=0.25,(\xi_0)_2=0.25$.

The functions $w_\pm$ and w_i depend on ξ_2. However, since ξ_2 plays the role of a parameter, this dependence is not written on the l.h.s. of the equations in (6.13). The center and the momentum of the initial Gaussian wave packet are given by (6.8).

6.4.1 The two dimensional surface hopping algorithm

The x_2-independent solutions to the surface hopping algorithm presented in Section 4 are obtained by replacing the system (2.14) with its two dimensional version:

$$\partial_t w_\pm \pm \frac{\xi_1}{|\xi|}\partial_{x_1} w_\pm - \alpha\partial_{\xi_1} w_\pm = 0, \quad \xi_1 \neq 0. \tag{6.14}$$

More precisely, Eq. (6.14) is used for the time evolution of $w_\pm$ as long as the classical trajectories $\varphi_t^\pm(x_1,\xi_1)$ solution to (5.6) are away from the hopping surface $\{\xi_1=0\}$. Then, the hopping transport is described as follows.

Consider an initial set of sampling points

$$\{(x_{1,k},\xi_{1,k},+)\in IR_{x_1}\times IR_{\xi_1}\times\{-,+\};\ k=1,\cdots,N\},$$

with associated weights $w_k\in IR$ given by:

$$w_k = w_+(0,x_{1,k},\xi_{1,k}).$$

For $t \geq 0$ small enough:

$$(x_{1,k}(t),\xi_{1,k}(t)) = \varphi_t^+(x_{1,k},\xi_{1,k}), \quad w_k(t) = w_k,$$

where, using (5.6), we have $\xi_{1,k}(t) = \xi_{1,k} - \alpha t$. Then, for $k = 1,\cdots,N$, if $0 < \frac{\xi_{1,k}}{\alpha} < t_f$, the classical trajectory is such that $\xi_{1,k}(t^*) = 0$ at the time $t^* = \frac{\xi_{1,k}}{\alpha}$ and non-adiabatic transfer occurs. For such a k, the weight is changed such that for $t > t^*$

$$w_k(t) = (1 - T^*) w_k(t^*),$$

and a new particle is created on the lower band with index $l > N$. For the new particle, the associated weight is such that for $t > t^*$

$$w_l(t) = T^* w_k(t^*).$$

In the above equations, the transition rate T^* is equal to:

$$T^* = e^{-\frac{\pi\xi_2^2}{h|\alpha|}}.$$

The surface hopping level populations at the final time t_f are then given by:

$$P^h_{sh,+}(t_f) = \sum_{k=1}^{N} w_k(t_f)\Delta x_1 \Delta\xi_1, \quad P^h_{sh,-}(t_f) = \sum_{l=N+1}^{M} w_l(t_f)\Delta x_1 \Delta\xi_1, \tag{6.15}$$

where Δx_1 and $\Delta\xi_1$ are the mesh sizes in the x_1 and ξ_1 directions respectively.

6.4.2 Comparison with the models in [30]

For Eqs. (5.2) and (5.3), the simulation domain is:

$$(x_1,\xi_1) \in \left[-11\sqrt{h}, 11\sqrt{h}\right] \times \left[(\xi_0)_1 - \alpha t_f - 5\sqrt{h}, (\xi_0)_1 + 5\sqrt{h}\right].$$

They are solved with periodic boundary conditions on a uniform grid with 500 points in the x_1-direction and 500 points in the ξ_1-direction. The time step size is chosen such that the condition of stability of the upwind method is satisfied [27]. More precisely, we take:

$$\Delta t = \left(\frac{1}{\Delta x_1} + \frac{\alpha}{\Delta\xi_1}\right)^{-1}.$$

Eqs. (5.2) and (5.3) are solved using a time-splitting method where the free equation (without source term) is solved using a dimensional splitting: the free problem is splitted in two one-dimensional problems and each one dimensional problem is solved using the one-dimensional second order upwind MUSCL scheme (see [27]). The source term is integrated in time using a RK2 method for Eq. (5.2) (in order to preserve the second order accuracy) and exactly for Eq. (5.3).

For Eq. (5.2), we take:

$$w_i|_{t=0}=0$$

in addition to the initial condition (6.13). We remark that, since the MUSCL method is written for real valued functions, the third equation in (5.2) has to be splitted in two equations, one for the real part of w_i and one for its imaginary part.

The level populations provided by the asymptotic model are defined by:

$$P^h_{am,\pm}(t)=\int_{IR^2} w_\pm(t,x_1,\xi_1)dx_1d\xi_1,$$

where $w_\pm$ is the solution to (5.2) and the level populations provided by the effective model are defined by:

$$P^h_{em,\pm}(t)=\int_{IR^2} w_\pm(t,x_1,\xi_1)dx_1d\xi_1,$$

where $w_\pm$ is the solution to (5.3). For the level populations $P^h_{sh,\pm}(t_f)$ defined in (6.15), the initial sampling is chosen as follows. We consider a uniform $J\times K$ discretization of the domain of the (x_1,ξ_1) variables:

$$[a,b]\times[c,d],$$

where $a=(x^h_0)_1-5\sqrt{h}$, $b=(x^h_0)_1+5\sqrt{h}$ and $c=(\xi_0)_1-5\sqrt{h}$, $d=(\xi_0)_1+5\sqrt{h}$. The grid points $(x_{1,j},\xi_{1,k})$, $j=1,\cdots,J$, $k=1,\cdots,K$ are ordered such that:

$$w_+(0,x_{1,1},\xi_{1,1})\geq\cdots\geq w_+(0,x_{1,J\times K},\xi_{1,J\times K}),$$

and we determine the minimal integer N such that:

$$\sum_{k=1}^{N} w_+(0,x_{1,k},\xi_{1,k})\Delta x_1\Delta\xi_1\geq 1-\text{tol},$$

where $\Delta x_1=\frac{b-a}{J}$, $\Delta\xi_1=\frac{d-c}{K}$ and tol is a well chosen tolerance. Then, the initial sampling is the set:

$$\{(x_{1,k},\xi_{1,k},+)\in IR_{x_1}\times IR_{\xi_1}\times\{-,+\};\ k=1,\cdots,N\}.$$

For all the tests in this section, the number of grid points for the two dimensional surface hopping algorithm is:

$$J=100,\quad K=100,$$

and the tolerance is

$$\text{tol}=10^{-9}.$$

We depict in Fig. 10 the time evolution of the level populations provided by the asymptotic model (5.2) and the two dimensional surface hopping algorithm. The curve with title Upper level am, resp. Lower level am, refers to $P^h_{am,+}(t)$, resp. $P^h_{am,-}(t)$. The total population, curve titled Total am, corresponds to $P^h_{am,+}(t)+P^h_{am,-}(t)$. The same is

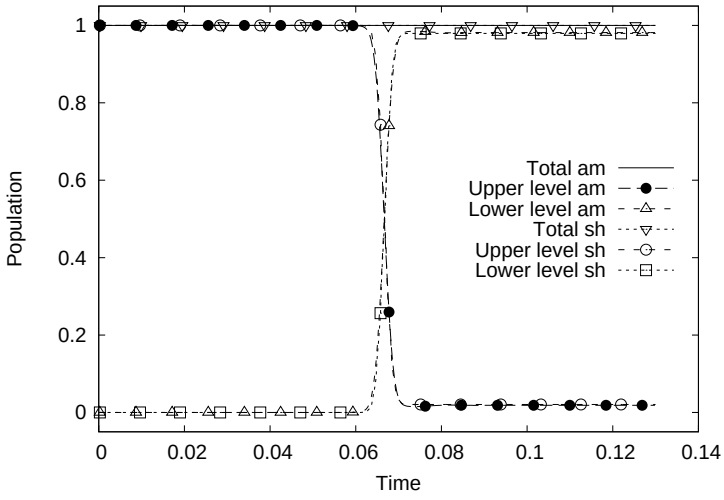

Figure 10: For $h=10^{-3}$, $\xi_2=10^{-2}$ and $U=\alpha x_1$, $\alpha=15$: time evolution of the level populations provided by the asymptotic model (5.2) and the two dimensional surface hopping algorithm presented in Section 6.4.1.

true when am is replaced by sh. The surface hopping curves are obtained by repeating the surface hopping algorithm described in Section 6.4.1 for the sequence of times $t_f = 0.13n/500$, $1 \leq n \leq 500$. The behavior is the same as in Section 6.2: the charge is initially carried completely by the upper level, then hopping occurs at time $t = 0.0667$ and the great majority of the charge is transferred to the lower level. The time evolution of the level populations provided by the asymptotic model fits well the one provided by the two dimensional surface hopping: the surface hopping algorithm validates the model (5.2).

Fig. 11 shows that non-adiabatic transfer is only partially recovered by model (5.3). We depict the time evolution of the level populations provided by the asymptotic model (5.3) and the two dimensional surface hopping algorithm where the transition probability T^* is replaced by (5.18), (5.5). The curve with title Upper level em, resp. Lower level em, refers to $P^h_{em,+}(t)$, resp. $P^h_{em,-}(t)$. The total population, curve titled Total em, corresponds to $P^h_{em,+}(t)+P^h_{em,-}(t)$. The same is true when em is replaced by sh. As in Fig. 10, hopping occurs at time $t = 0.0667$. However, using the simplified model (5.3), only about a half of the charge is transferred to the lower level which is close to the transition probability given by (5.18), (5.5) and substantially different from Fig. 10.

In Fig. 12, we verify numerically that the transition probability corresponding to the effective model (5.3) is given by the formula (5.18). The curve with title Trans eff refers to $P^h_{em,-}(t_f)$, the population provided by the effective model (5.3) on the lower level and at the final time, for 31 different values of the constant β distributed uniformly on the interval [0,5]. The constant β given by (5.5) is made arbitrary in (5.18) by replacing the coefficient τ appearing in (5.3) by $\tilde{\tau} = \frac{\beta}{\pi^2/4}\tau$. The curve with title Trans th is the representation of the coefficient T given by (5.18) for the same values of β. We remark that the

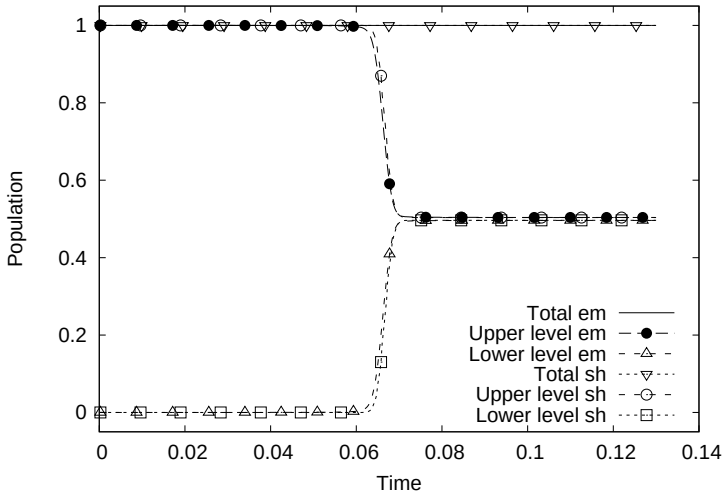

Figure 11: For $h=10^{-3}$, $\xi_2=10^{-2}$ and $U=\alpha x_1$, $\alpha=15$: time evolution of the level populations provided by the effective model (5.3) and the two dimensional surface hopping algorithm presented in Section 6.4.1 where the transition probability T^* is replaced by (5.18), (5.5).

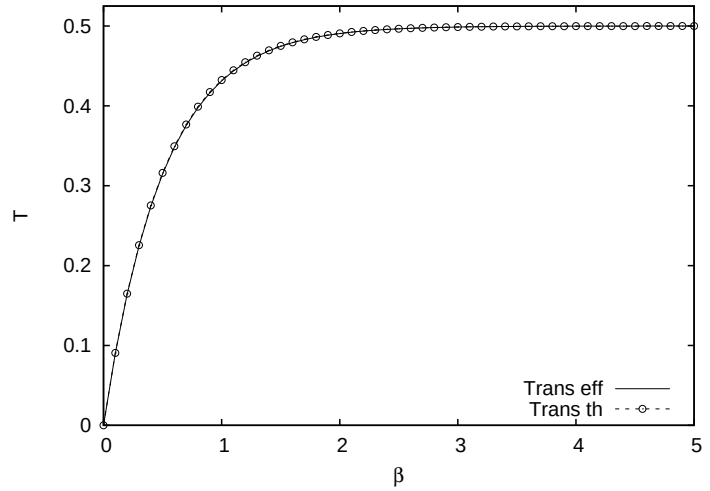

Figure 12: For $h=10^{-3}$, $\xi_2=10^{-2}$, $t_f=0.13$ and $U=\alpha x_1$, $\alpha=15$: numerical verification of the formula (5.18) for the transition probability corresponding to the model (5.3).

two curves are very close which validates the limit $\xi_2 \to 0$ performed in Section 5 for the solution to (5.3).

In the present section, the fact that (5.2) is found to be correct, at least for the example in question, is a significant finding in itself. In particular, it does not follow by the standard Wigner measures theory.

Appendix

A Time-splitting spectral method (TSSM)

The solution $u(t,x)$ to (2.6) is computed on the domain:

$$\Omega=[a_1,b_1]\times[a_2,b_2]$$

using a time-splitting spectral method as in [18]. For $r=1,2$, we choose the spatial mesh size $\Delta x_r=\frac{b_r-a_r}{N_r}$ in the r direction for a given integer N_r. Define a uniform grid

$$x_j=a+(j_1\Delta x_1,j_2\Delta x_2),\quad j\in\mathcal{J}, \tag{A.1}$$

where

$$\mathcal{J}=\{j=(j_1,j_2)\in\mathbb{N}^2\,|\,0\le j_1<N_1,0\le j_2<N_2\}$$

and $a=(a_1,a_2)$. For a given time step size Δt, let u_j^n denote the numerical approximation of $u(t^n,x_j)$ at the time $t^n=n\Delta t$, $n\ge 0$. Then, u_j^{n+1} is computed from u_j^n by decomposing the problem (2.6) in the two sub-problems

$$ih\partial_t u=[-ih\sigma_1\partial_{x_1}-ih\sigma_2\partial_{x_2}]u \tag{A.2}$$

and

$$ih\partial_t u=Uu. \tag{A.3}$$

The free Dirac equation (A.2) is solved using a spectral method in space and exact time integration, whereas Eq. (A.3) can be integrated exactly on $[t^n,t^{n+1}]$. To discretize (A.2), we introduce the trigonometric interpolant of u:

$$\tilde{u}(t,x)=\frac{1}{N_1N_2}\sum_{k\in\mathcal{K}}\widehat{u(t)}_k e^{i\xi_k\cdot(x-a)}, \tag{A.4}$$

where $\tilde{u}(t,x_j)=u(t,x_j)$. In Eq. (A.4), we have

$$\mathcal{K}=\left\{k=(k_1,k_2)\in\mathbb{Z}^2\,\Big|\,-\frac{N_1}{2}\le k_1<\frac{N_1}{2},-\frac{N_2}{2}\le k_2<\frac{N_2}{2}\right\}$$

and

$$\xi_k=2\pi\left(\frac{k_1}{b_1-a_1},\frac{k_2}{b_2-a_2}\right).$$

For a given function $f:IR^2\to\mathbb{C}^2$, $\hat{f}_k$ is the discrete Fourier transform (DFT) of f defined by

$$\hat{f}_k=\sum_{j\in\mathcal{J}}f_j e^{-i\xi_k\cdot(x_j-a)}, \tag{A.5}$$

where $f_j = f(x_j)$. When $f = (f_j)_{j\in\mathcal{J}}$ is a sequence with $f_j \in \mathbb{C}^2$, the DFT of f is the sequence $\hat{f}_k$ defined by Eq. (A.5). Inserting (A.4) into (A.2), and using the orthogonality of the set $\left\{e^{i\xi_k\cdot(x-a)},\ k\in\mathcal{K}\right\}$ with respect to the scalar product of $L^2(\Omega)$, one gets the following system of ODE

$$\frac{d}{dt}\widehat{u(t)}_k = -iB(\xi_k)\widehat{u(t)}_k.$$

For any $t_0 \in IR$, the exact solution to the previous equation is given by:

$$\widehat{u(t)}_k = M(t-t_0,\xi_k)\widehat{u(t_0)}_k,$$

where

$$M(\delta,\xi) = e^{-i\delta B(\xi)}.$$

Applying an inverse discrete Fourier transform, one obtains the following expression for the approximation $u(t)_j$ of $u(t,x_j)$:

$$u(t)_j = \frac{1}{N_1N_2}\sum_{k\in\mathcal{K}} M(t-t_0,\xi_k)\widehat{u(t_0)}_k e^{i\xi_k\cdot(x_j-a)}.$$

We remark that using the eigenvectors (2.9), the matrix $B(\xi)$ can be diagonalized as follows:

$$B(\xi) = P(\xi)D(\xi)P(\xi)^*,$$

where

$$D(\xi) = \mathrm{diag}\left(|\xi|,-|\xi|\right), \quad P(\xi) = (\chi_+(\xi),\chi_-(\xi))$$

and therefore

$$M(\delta,\xi) = P(\xi)e^{-i\delta D(\xi)}P(\xi)^* = \begin{pmatrix} \cos(\delta|\xi|) & -i\sin(\delta|\xi|)(\xi_1-i\xi_2)/|\xi| \\ -i\sin(\delta|\xi|)(\xi_1+i\xi_2)/|\xi| & \cos(\delta|\xi|) \end{pmatrix}. \tag{A.6}$$

The Strang splitting is the second order method constructed as follows: solve the first subproblem (A.2) over only a half time step of length $\frac{\Delta t}{2}$. Then, we use the result as data for a full time step on the second subproblem (A.3) and finally take another half time step on (A.2). This leads to the following method:

$$\begin{aligned} u_j^* &= \frac{1}{N_1N_2}\sum_{k\in\mathcal{K}} M(\Delta t/2,\xi_k)\widehat{(u^n)}_k e^{i\xi_k\cdot(x_j-a)}, \\ u_j^{**} &= e^{-\frac{i}{\hbar}U_j\Delta t}u_j^*, \\ u_j^{n+1} &= \frac{1}{N_1N_2}\sum_{k\in\mathcal{K}} M(\Delta t/2,\xi_k)\widehat{(u^{**})}_k e^{i\xi_k\cdot(x_j-a)}. \end{aligned} \tag{A.7}$$

Remark A.1. It follows directly from the unitarity of the DFT and of the matrix $M(\delta,\xi)$ given by (A.6) that the TSSM (A.7) conserves the discrete total charge, i.e.:

$$\|u^n\|_2 = \|u^0\|_2, \quad \forall n \geq 0, \tag{A.8}$$

where the norm $\|.\|_2$ is defined in (6.6). Moreover, when the potential is equal to a constant $U = U_0$, the Dirac equation (2.6) admits the following plane wave solutions:

$$u(t,x) = \chi_{\pm}(k) e^{\frac{i}{h}(k.x-(U_0 \pm |k|)t)},$$

which are integrated exactly by the TSSM (A.7) if $k \in I\!R^2$ satisfies $\frac{k}{h} = \xi_{k'}$ for some $k' \in \mathcal{K}$. In the case of the Schrödinger equation, an analysis of the stability of the TSSM was performed in [8] for initial conditions which are close to plane waves.

B Discussion on the accuracy of the TSSM

The Dirac equation (2.10) is solved using the TSSM presented in Section A. The potential U, the initial condition and the simulation domain are as in Section 6.2. The final time is $t_f = 0.13$.

The accuracy of solutions given in the second line of Table 3 represents the L^2-norm difference:

$$\|u^h(t_f,.) - \tilde{u}^h(t_f,.)\|_{L^2} \tag{B.1}$$

of the final reference solution $u^h(t_f,.)$ and a coarser solution $\tilde{u}^h(t_f,.)$. The number of space points is given by $(N_1,N_2) = (1024,512)$ for the reference solution and $(N_1,N_2) = (256,128)$ for the coarser solution, except for $h = 10^{-4}$ where the number of space points is given by $(N_1,N_2) = (2048,1024)$ for the reference solution and $(N_1,N_2) = (1024,512)$ for the coarser solution. The number of time steps is fixed as 10^4. Since it is the square of the L^2-norm which is relevant for the computation of the level populations, the accuracy for $h = 10^{-2}$ and 10^{-3} is close to the machine precision. For the other values of h the TSSM is accurate enough for the validation of the surface hopping algorithm whose methodological error is of the order of $\sqrt{h}$.

Table 3: At time $t_f = 0.13$: accuracy of the TSSM for different values of the semiclassical parameter h.

h	10^{-1}	10^{-2}	10^{-3}	10^{-4}
Accuracy	1.55×10^{-4}	4.74×10^{-8}	6.62×10^{-6}	4.64×10^{-3}

In Table 4, the accuracy is given by Eq. (B.1) where the reference solution $u^h(t_f,.)$ is computed with 10^5 time steps and $\tilde{u}^h(t_f,.)$ is a less resolved solution computed with various numbers of time steps. The number of space points is fixed as $(N_1,N_2) = (1024,512)$. The solution with 10^4 time steps is accurate enough for our purpose and takes $12202.94s$ computing.

Table 4: At time $t_f = 0.13$ and for $h = 10^{-2}$: accuracy of the TSSM for different values of the number of time steps.

Time steps	10^4	10^3	10^2
Accuracy	7.70×10^{-3}	8.47×10^{-2}	0.83

Remark B.1. Since the simulation time t_f is h-independent (this is imposed by the fact that the hopping time is h-independent) and the size of the simulation box Ω tends to 0 when h tends to 0, the solution of the Dirac equation (2.6) will reach the boundary of Ω for small values of h. Therefore, in addition to the periodic boundary conditions provided by the spectral method, absorbing boundary layers can be used at the edge of the simulation box, see e.g. [34]. We remark that, although it is not applied in the present work, such boundary layers provide an improvement of the performance of the TSSM in the case $h = 10^{-4}$.

Acknowledgments

This research is supported by NSFC grant 91330203, NSF grants 1114546, 1522184 and 1107291 "RNMS: KI-Net".

A.F. acknowledges Clotilde Fermanian Kammerer for discussion about Section 3.3.

References

[1] A. Athanassoulis, T. Katsaounis, I. Kyza, Regularized semiclassical limits: linear flows with infinite Lyapunov exponents, Commun. Math. Sci. 14 (2016) 1821-1858.
[2] C. W. Beenakker, Colloquium: Andreev reflection and Klein tunneling in graphene, Rev. Mod. Phys. 80 (2008) 1337.
[3] V. Bonnaillie-Noël, A. Faraj, F. Nier, Simulation of resonant tunneling heterostructures: numerical comparison of a complete Schrödinger-Poisson system and a reduced nonlinear model, J. Comput. Electron. 8, 1 (2009) 11-18.
[4] D. Brinkman, C. Heitzinger, P. A. Markowich, A convergent 2D finite-difference scheme for the Dirac-Poisson system with magnetic potential and the simulation of graphene, J. Comput. Phys. 257, A (2014) 318-332.
[5] A. H. Castro Neto, F. Guinea, N. M. R. Peres, K. S. Novoselov, A. K. Geim, The electronic properties of graphene, Rev. Mod. Phys. 81, 1 (2009) 109-162.
[6] L. Chai, S. Jin, Q. Li, O. Morandi, A Multiband Semiclassical Model for Surface Hopping Quantum Dynamics, SIAM Multiscale Model. Simul. 13, 1 (2015) 205-230.
[7] K. Drukker, Basics of surface hopping in mixed quantum/classical simulations, J. Comp. Phys. 153 (1999) 225-272.
[8] E. Faou, L. Gauckler and C. Lubich, Plane Wave Stability of the split-step Fourier method for the nonlinear Schrödinger equation, Forum Math. Sigma 2, e5 (2014) 45 pp.
[9] C. Fermanian Kammerer, P. Gérard, A Landau-Zener formula for non-degenerated involutive codimension three crossings, Ann. Henri Poincaré 4 (2003) 513-552.

[10] C. Fermanian Kammerer, P. Gérard, Mesures semi-classiques et croisements de mode, Bull. S.M.F 130, 1 (2002) 123-168.
[11] C. Fermanian Kammerer, F. Méhats, A kinetic model for the transport of electrons in a graphene layer, hal-01160791.
[12] G. Fiori, G. Iannaccone, Simulation of Graphene Nanoribbon Field-Effect Transistors, IEEE Electron. Device Lett. 28, 8 (2007) 760-762.
[13] P. Gérard, P. A. Markowich, N. J. Mauser, F. Poupaud, Homogenization Limits and Wigner Transforms, Comm. Pure Appl. Math. 50, 4 (1997) 323-379.
[14] V. Grecchi, A. Martinez, A. Sacchetti, Destruction of the beating effect for a non-linear Schrödinger equation, Commun. Math. Phys. 227, 1 (2002) 191-209.
[15] G. A. Hagedorn, Proof of the Landau-Zener formula in an adiabatic limit with small eigenvalue gaps, Commun. Math. Phys. 136 (1991) 433-449.
[16] R. Hammer, W. Pötz, A. Arnold, Single-cone real-space finite difference scheme for the time-dependent Dirac equation, J. Comput. Phys. 265 (2014) 50-70.
[17] L. Hörmander, The Analysis of Linear Partial Differential Operators. III. Pseudodifferential Operators, Grundlehren der Mathematischen Wissenschaften [Fundamental Principles of Mathematical Sciences] No. 274, Springer-Verlag, Berlin, 1985.
[18] Z. Huang, S. Jin, P. A. Markowich, C. Sparber, C. Zheng, A time-splitting spectral scheme for the Maxwell-Dirac system, J. Comput. Phys. 208 (2005) 761-789.
[19] S. Jin, Runge-Kutta methods for hyperbolic conservation laws with stiff relaxation terms, J. Comput. Phys. 122 (1995) 51-67.
[20] S. Jin, P. A. Markowich, C. Sparber, Mathematical and computational methods for semiclassical Schrödinger equations, Acta Numerica 20 (2011) 121-209.
[21] S. Jin, K. Novak, A coherent semiclassical transport model for pure-state quantum scattering, Comm. Math. Sci. 8 (2010) 253-275.
[22] S. Jin, P. Qi, A Hybrid Schrödinger/Gaussian Beam Solver for Quantum Barriers and Surface Hopping, Kinetic and Related Models 4 (2011) 1097-1120.
[23] S. Jin, P. Qi, Z. Zhang, An Eulerian surface hopping method for the Schrödinger equation with conical crossings, Multiscale Model. Simul. 9, 1 (2011) 258-281.
[24] C. Lasser, T. Swart, S. Teufel, A rigorous surface hopping algorithm for conical crossings, Commun. Math. Sc. 5, 4 (2007) 789-814.
[25] C. Lasser, S. Teufel, Propagation through conical crossings: an asymptotic semigroup, Comm. Pure Appl. Math. 58, 9 (2005) 1188-1230.
[26] M. C. Lemme, T. J. Echtermeyer, M. Baus, H. Kurz, A Graphene Field-Effect Device, IEEE Electron. Device Lett. 28, 4 (2007) 282-284.
[27] R. J. LeVeque, Finite Volume Methods for Hyperbolic Problems, Cambridge University Press, Cambridge, 2002.
[28] O. Morandi, Multiband Wigner-function formalism applied to the Zener band transition in a semiconductor, Physical Review B 80, 2 (2009) 024301-024312.
[29] O. Morandi, F. Schürrer, Wigner model for Klein tunneling in graphene, Communications in Applied and Industrial Mathematics 2, 1 (2011).
[30] O. Morandi, F. Schürrer, Wigner model for quantum transport in graphene, J. Phys. A: Math. Theor. 44 (2011) 265301.
[31] D. S. Novikov, Elastic scattering theory and transport in graphene, Phys. Rev. B 76 (2007) 245435.
[32] K. S. Novoselov, A. K. Geim, S. V. Morozov, D. Jiang, Y. Zhang, S. V. Dubonos, I. V. Gregorieva, A. A. Firsov, Electric Field Effect in Atomically Thin Carbon Films, Science 306,

5696 (2004) 666-669.
[33] L. Pareschi, Central Differencing Based Numerical Schemes for Hyperbolic Conservation Laws with Relaxation Terms, SIAM J. Numer. Anal. 39, 4 (2001) 1395-1417.
[34] U. W. Rathe, C. H. Keitel, M. Protopapas, P. L. Knight, Intense laser-atom dynamics with the two-dimensional Dirac equation, J. Phys. B 30, 15 (1997) L531-L539.
[35] D. Sholl and J. Tully, A generalized surface hopping method, J. Chem. Phys. 109 (1998) 7702-7710.
[36] C. Sparber, P. A. Markowich, Semiclassical asymptotics for the Maxwell-Dirac system, J. Math. Phys. 44, 10 (2003) 4555-4572.
[37] B. Thaller, The Dirac Equation, Springer, New York, 1992.
[38] J. Tully, Molecular dynamics with electronic transitions, J. Chem. Phys. 93 (1990) 1061-1071.
[39] J. Tully, R. Preston, Trajectory Surface Hopping Approach to Nonadiabatic Molecular Collisions: The Reaction of H^+ with D_2, J. Chem. Phys. 55 (1971) 562-572.
[40] C. Zener, Non-adiabatic crossing of energy levels, Proc. Royal. Soc. London Ser. A 137 (1932) 696-702.